DOE/ET/13390--T2

IRON-AIR BATTERY DEVELOPMENT PROGRAM

E. S. Buzzelli, C. T. Liu, W. A. Bryant

Interim Report 1978

Contract No. DE-AC02-76ET13390
formerly EY-76-C-02-2949

May 1980

MASTER

Westinghouse R&D Center
1310 Beulah Road
Pittsburgh, Pennsylvania 15235

TABLE OF CONTENTS

		Page
I.	Summary	1-1
II.	Introduction	2-1
III.	Air Electrode Studies	3-1
	3.1 Introduction	3-1
	3.2 Experimental Results	3-1
	3.3 Discussion of Results	3-5
IV.	Iron Electrode Studies	4-1
	4.1 Introduction	4-1
	4.2 Procedure	4-7
	4.3 Experimental Results	4-8
	4.3.1 Fe_2O_3 Powder Studies	4-8
	4.3.2 Fe Powder Activation Studies	4-12
	4.3.3 Optimization of Fe Electrode's Density and Thickness	4-26
	4.3.4 Fe Electrode Characterization	4-28
	4.3.5 Continuing Efforts Toward Electrode Improvement	4-35
	4.4 Discussion of Results	4-43
	4.4.1 Iron Powder Activation	4-43
	4.4.2 Effect of Sintering Parameters	4-44
	4.5 Summary	4-51
V.	Cell Studies	5-1
	5.1 Cell Testing Program	5-1
	5.2 Cell Testing	5-2
	5.3 Cell Test Results	5-3
	5.4 Module Design and Testing	5-11
	5.5 Energy Efficiency of Iron-Air Cells	5-12
VI.	Appendix	6-1
	6.1 Iron Electrode Model	6-1
VII.	References	7-1

ABSTRACT

This report describes the research and development efforts of the program at the Westinghouse Electric Corporation on Iron-Air Batteries during the period June 1977 - May 1978. This battery is being developed as an advanced battery system for electric-vehicle propulsion. Objectives for both electrodes and cells have been established to be compatible with a final fully-engineered battery which will ultimately store greater than 140 wh/kg and deliver greater than 100 w/kg. Work during this portion of the program has emphasized the cell testing aspects of the iron-air system along with individual electrode improvement. The cyclic voltage efficiency of 100 cm^2 size cells has been shown to be in excess of 50% with individual iron and air electrode performance characteristics comparable or superior to those characteristics established in the half cell testing program.

Long-term cyclic stability for greater than 100 cycles has been established for several 100 cm^2 size cells. Work, presently underway, and tests planned in the near future, are expected to demonstrate the near-term expected performance characteristics of the iron-air cells. Additional studies are underway to improve the performance characteristics of the individual electrodes through improved processing procedures and to incorporate these improvements into the cell test program.

I. SUMMARY

This interim report describes the progress and work which has been carried out on the Iron-Air Development Program for the period June 1977 - May 1978. The work described covers cell studies and experiments on both the iron and air electrode to improve their individual performance characteristics. Test results are also presented for tests carried out in 100 cm^2 pre-prototype size iron-air cells with cyclic performance for greater than 100 cycles.

Increased emphasis during this work period has been placed on the hardware and cell development portion of the program to demonstrate cell characteristics of voltage efficiency, energy efficiency, power capability and cyclic stability. Work during this time period has continued to advance the performance and life of 100 cm^2 size cells while incorporating and evaluating cell design and assembly procedures to permit the extended life testing of pre-prototype 100 cm^2 size cells. Improved air and iron electrodes have also been utilized in the cell tests to determine their characteristics under cell conditions.

II. INTRODUCTION

The iron-air system offers many advantages over other systems considered as candidate battery systems for vehicle propulsion. This ambient temperature system has the potential for providing a high energy density power source with long life at low cost. There are, however, obstacles to be overcome, foremost of which is the life requirement of 1000° deep discharge cycles. Progress has been made as evidenced by the long life (>300 cycles) already achieved by the Westinghouse low cost, bifunctional air electrodes. High capacity, low cost iron electrodes prepared by the press and sinter technique have shown great promise for achieving a metal-air system capable of meeting the ultimate objectives of this development program.

The ultimate performance goals for the ambient temperature, secondary Iron-Air Battery Systems are:

140 whr/kg	Energy Content
100 w/kg	Power Capability
$30/kwh	Manufacturing Cost
1000 cycles	Life
60%	Energy Efficiency

Further progress toward meeting the objectives and goals for the iron-air battery system are described in the following sections of this interim report for the period June 1977 - May 1978.

III. AIR ELECTRODE STUDIES

3.1 Introduction

It was discovered, as a result of our previous studies (June 1976 - June 1977)*, that the discharge performance of an air electrode was primarily dependent upon its wetting characteristics. It has also been learned that proper wetting is associated with the formation of many small cracks and that this preferred structure can be achieved by the dry powder processing technique which has supplemented the technique of wet pasting. To date, this emphasis on the structural aspects rather than the chemistry, and chemicals of the air electrode has provided us with electrodes which exhibit both increased discharge potential and reduced break-in period.

Emphasis has also been given to the life testing of full iron-air cells, each containing two 100 cm^2 air electrodes designed to demonstrate acceptable performance for a minimum of 100 cycles. A total of 75 such cells have been constructed. The first 30 cells were used to establish the assembly and test procedure along with the experimental setup. The goal of 100 cycles has been reached in several cells.

Additional studies included those on the charge potential of the air electrode and those evaluating failure mode.

3.2 Experimentation and Test Results

It has been mentioned previously that the desirable "mud-caking" of the electrode as a result of the wet-pasting technique was responsible for a proper distribution of the wetting agent in Teflon 30B into the most favorable morphology*. In order to test this hypothesis (as well as to improve the air electrode's performance) a new method of electrode preparation was initiated. Three active materials, each intended to fulfill a specific

---

*Iron-Air Battery Development
Interim Report June 1976 - June 1977, COO/2949-1 January 1978.

function, were individually prepared. The first, identified by the letter C, was prepared to carry the full current load during the charging mode, whereas, the second material, designated by the letter D, was intended to carry the current load of the discharge cycle. The third active material, designated by the letter A, was a simple mix of carbon and Teflon 30B (with the ratio of 100 parts carbon to 45 parts Teflon 30B) with a large excess of water, which was filtered, washed and then finally air dried.

The first mixture of C material (C-1) consisted of 100g of carbon, 5.3g of colloidally precipitated silver, 35g of Teflon 30B, 25g of WC-12 w/o Co and approximately 800g of water. This paste was spread onto a large plastic screen (with approximately 1/16" square openings) and permitted to dry in air. The D-1 active material was a mixture of 105.3g of silverized carbon, 45g of Teflon 30B and about 800g of water. However, in an attempt to increase the discharge performance, an additional wetting agent (Triton X-100) was added to bring the mixture to the equivalent of a carbon to Teflon 30B ratio of 10 to 7 in terms of the quantity of wetting agent. The lower ratio material was used as the layer closer to the air side. On the air side, a class A material containing only a residual amount of wetting agent was applied.

The compositions of active materials used in 75 cm^2 size air electrodes are shown in Tables I-A and I-B. Combinations of various active materials were placed into a specific layer of the electrode as shown in Tables II-A and II-B.

The electrical performance characteristics of electrodes prepared by this manner have shown predictable results in half-cell testing. Two unexpected results included short cycle life and a rather short duration of good charge-discharge performance before the performance started to deteriorate. However, as a result of these tests (LU-21 to -26), we learned that a proper wettable region was responsible for the good discharge performance and that localized unwettable portions were required to lower the charging potential. The results of charge-discharge performance characteristics of these electrodes are included in Table III-A and IV-A.

A homogeneous mixture of C and D materials (DC material) was prepared in a wet mix and dried. Electrodes (such as LU-27 to -29) prepared from this material showed rather poor performance in the discharge mode but exhibited low charge potentials. These results confirmed the conclusion of the tests on the carbon-Teflon 30B mixtures, i.e., that higher ratios of carbon to Teflon 30B produced poor performance. The results also indicate that, with identical mixtures of active materials, electrodes made by the wet pasting technique perform better than those made by the homogeneously mixed dry powder preform method of mechanical fabrication.

Electrodes LU-30 to LU-34 were prepared from a mixture of Shawinigan black with a new highly conductive, high surface area carbon (Ketjenblack). Rather poor results were observed on the first four electrodes tested, while the fifth electrode, LU-34, showed somewhat promising performance as shown in Table III-A.

The half cell, LU-035, was prepared by wet pressing of the C-4E material between two nickel fiber plies followed by overnight air drying. Four such plaques were made. Some C-4E material was then wet pasted on each side of the plaques. After being air dried the plaques were pressed together. This electrode showed good performance in both charge and discharge cycles. However, this result simply proved that, with proper preparation, wet pasting of C-4E material produces a good air electrode. This had been known before. Since this electrode did not yield any further specific information, its half cell testing was terminated.

Air electrode LU-036 was made in a manner identical to those air electrodes made for 100 cm^2 size full cells (cells #31 and #32) and tested. The active materials used in this cell were similar to the C-4E formula with employment of a modified Teflon 30B content for each layer acting as a means of controlling the wetting characteristics. In theory, this electrode should perform considerably better than the previous one (LU-035), at least on discharge. However, the result was found to be contrary to our expectation. The reason for this will be discussed later. Once again the irreproducible nature of the wet pasting technique has been demonstrated.

Electrodes LU-037 and LU-038 were designed to test the effect of lower Teflon 30B and FEP contents on the charge-discharge performance. Since it had been learned previously that a lower Teflon content always gave poor performance (due to poor wetting of the electrode), additional wetting agent, Triton X-100, was added to make up the difference in terms of hydrophilicity. In the C-4E formula, the ratio of carbon to Teflon 30B is 12/4.2, whereas in the B01 (Table I-A) composition, the ratio is 12/2.0. There is a difference of 2.2g of Teflon 30B between the two, and that difference in terms of wetting agent content was made up by substitution of Triton X-100. Teflon 30B emulsion contains 6 w/o of Triton X-100. Therefore, 2.2 x 0.06 = 0.132g of Triton X-100 was required. The dilute Triton X-100 solution made up as stock solution contains 1.7g of Triton X-100 in 500 ml. Thus, 30 ml of this silute solution is equivalent to 0.1g of wetting agent. This means that B-1 mix in Table I-A will have a hydrophilic nature similar to a blend containing the ratio of carbon to Teflon 30B of 12/3.7 or 9/2.8, which is greater than those of blends #5 (1502) which is 12/4.4, or C-4E formula which is 9/3.15. And yet, the discharge performance of both electrodes, LU-037 and LU-038, can be considered as among the best ever tested. The only difference between the two electrodes was in the amount of active material loaded on each plaque. As shown in Table II-B, electrode LU-038 contains approximately 10% more active material than LU-037.

To simulate the air electrode used in cell #68, electrode LU-039 was prepared for half cell testing. The active material used in this electrode was modified blend #5 which is shown in Table V-A. Although there was some improvement in the charging potential, the discharge performance was surprisingly poor. A set of five electrodes (LU-040, -041, -04s, -043 and -044) was prepared to test the effect of Teflon 30B content (in a mix prepared by wet pasting) on the discharge performance. Active materials, construction procedures and corresponding charge-discharge performances are included in Tables I-B, II-B, III-B and IV-B. Quite different results were obtained as compared with a dry powder method, i.e., there is an optimum content of Teflon 30B which is particularly favorable

to the wet pasting method of preparation. This optimum content of Teflon 30B in a paste should be somewhere around 10/3 in terms of the ratio of carbon to Teflon 30B.

Up to this point, the discharge characteristics of the air electrode have been fairly well established. Factors which affect the discharge potential have been identified and the directions of the effects recognized. Attention was then turned to the study of factors which effect the charging potential of an air electrode. Our discovery and application of catalysts, such as WC-12 w/o Co, $FeWO_4$, NiS, etc., has lowered the oxygen overvoltage of air electrodes from +.76V vs. Hg/HgO to +.58V at the same charging condition. However, in most cases, the charging voltages of air electrodes have been higher than +0.6V vs. Hg/HgO. Electrode LU-045, containing $NiSO_4 \cdot 4H_2O$ was prepared to test whether Ni-salt forms active Ni-hydroxide under the testing conditions. No effect on the charging potential was noticed. Sintered iron sponge was mixed in the active material. Electrodes LU-046 to LU-056 were prepared with essentially identical active material. Varied were the process, current collector type, number of plaques used in each electrode, load condition and method of iron powder application. These data are shown in Table II-B. The effect of the iron powder in the air electrode on the charging potential is obvious from the charging voltage results shown in Table IV-B. All of air electrodes containing the sponge iron powder, regardless of the method of application, exhibited much lower charging potential than the comparable electrode with no sponge iron.

3.3 Discussion

After the establishment of a model for the bifunctional air electrode, the accuracy of the model remained to be proven and demonstrated. The dry powder technique was modified to fabricate air electrodes as close to those of the model as possible. Initially, fourteen such air electrodes (LU-021 - 034) were prepared. It was found that these electrodes behaved as electrodes prepared by the wet pasting technique, and included some of their shortcomings such as premature leakage of electrolyte. Although most

of the electrodes have shown good discharge performance during their test life, they were, in general, short-lived. However, for the first time it has been confirmed that the model was correct and, at the same time, it has been shown that the wet pasting technique can be replaced and duplicated by a dry powder technology.

Studies on controlled "mud-caking" were carried out with 100 cm^2 air electrodes prepared for full cell testing*. Initial results indicated that there is an optimum size of "mud-cake" cracking which gives an air electrode optimum discharge performance. However, it was later concluded that this controlled "mud-caking" would not give us reliable results unless there is a way to measure and control the degree of fibrillation of the Teflon 30B. This is a formidable task since the phenomenon of fibrillation cannot be defined in either a simple manner or by a simple test.

With both electrodes prepared essentially with the C-4E formula, electrode LU-036 was designed to have improved discharge performance over that of electrode LU-035 by increasing the Teflon 30B content on the electrolyte side layer to render it more hydrophilic. However, the test result was contrary to our expectation. Hydrophilicity, due to wetting agent alone, could not explain this finding and other observations made during the study of controlled "mud-caking" as mentioned earlier. A separate experiment was carried out to establish the point that the greater the Teflon 30B content in the mix, the easier the mix is made to possess the appropriate hydrophilic property when the same pasting condition is applied. Special attention and care must be taken to increase the wetting characteristics of an air electrode made with the increased Teflon 30B content in the active paste.

In order to prove this point, two electrodes (LU-037 and -038) were made to investigate their discharge performances. The contents of both Teflon 30B and FEP were greatly reduced in these electrodes. However, Triton X-100 was added to supplement the deficient quantity of the wetting agent. Discharge performances improved greatly, as shown in Table III-B.

---

*See Figures 3 - 2, 3, and 4

As discussed earlier, in order to obtain the improved discharge performance of an air electrode by the wet-pasting technique, the ratio of carbon to Teflon 30B should be around 10 to 3 which coincides with the original C-4E formula. Blend No. 5 and other successful compositions for air electrode materials also contain this ratio. However, unlike electrodes made by the dry powder technique, the discharge performance of an air electrode made by the wet paste technique does not appear to be improved by increasing the Teflon 30B content alone in the active material. This was confirmed by a series of tests (LU-040 to -044). Of course, this conclusion cannot be valid if different paste thickness and different amounts of the paste are applied to each layer of plaque. Therefore, it becomes even more difficult to make reproducible air electrodes by the wet pasting method since the degree of Teflon 30B fibrillation has a greater effect on hydrophilicity in this application.

Additions of iron powder in the active materials has shown promise in reducing the charging potential of air electrodes (LU-046, -048 and LU-050 to -056). Iron has been known to have a lower oxygen overvoltage than most candidate current collectors. The proper application of this material addition to the active material has shown this effect in the initial electrode tests. More studies are planned and will be conducted in the future.

Many of the 75 cm^2 air electrodes tested in the past were disecated for a post-mortem examination to help determine the actual cause of failure. It was difficult to pinpoint the real or sole cause of the electrode failure because all electrodes, except the ones which were tested only for a short time due to poor performance, showed physical delamination or separation of layers within the electrode to some degree. At this time, we do not know whether this delamination of the individual layers is the cause or the result of the failure. Along with this type of gross separation, there are many smaller locations within the layers where delamination occurs with the current collector completely separated from carbon or still in contact with either front or back sides of the active material layer. Sometimes delamination

occurs on a small region of layers. Attempts to correlate the charge-discharge performance with the type of delamination resulted in poor and rather vague conceptual conclusions. Several approaches have been taken into consideration. The solution, for now, is to provide improved bonding within each active material layer.

Table 1-A

$75\ cm^2$ Air Electrode Active Materials

	A-1	A-2	B-1	B-2	C-1	C-2	D-1	D-2	DC-1	DC-2	DC-3	DC-4	DC-5
Shawinigan Black	50	10	12	12	100	60	100	60	100	50	50	80	50
Ketjenblack	--	--	--	--	--	--	--	--	--	--	50	20	50
FEP	--	--	2	2	--	--	--	--	40	20	40	40	--
Teflon 30B	22.5	3	2	2	35	22	45	27	45	17.5	35	35	40
$AgNO_3$	--	--	4	--	8.5	--	8.5	5.1	8.5	--	8.5	8.5	17
WC-12 w/o Co	--	--	4	--	25	14	--	--	33	10	33	33	33
$FeWO_4$	--	--	--	--	--	14	--	--	--	--	--	--	--
NiS	--	--	--	--	--	14	--	--	--	--	--	--	--
Triton X-100 (mℓ)	--	--	--	--	--	--	--	--	--	0.5	--	--	--
Dil. Triton X-100 (mℓ)	--	--	30	--	--	--	--	--	--	--	--	--	--
H_2O (mℓ)	--	--	45	70	--	--	--	--	--	--	--	--	--

Table 1-B

75 cm^2 Air Electrode Active Materials

	E-1	E-2	E-3	E-4	E-5	F-1	G-1	G-2	G-3
Shawanigan Black	10	10	10	10	10	6	10	10	10
FEP	--	--	--	--	--	--	2	2	2
Teflon 30B	2	3	3.5	4	5	1.8	2	2	2
$AgNO_3$	0.085	0.085	0.085	0.085	0.085	0.05	0.6	0.6	--
WC-12 w/o Co	--	--	--	--	--	--	4	3	--
NiS	--	--	--	--	--	--	6	3	--
$NiSO_4 \cdot 6H_2O$	--	--	--	--	--	4.8	--	--	--
Triton X-100	--	--	--	--	--	0.055	--	--	--
H_2O	60	60	60	60	60	40	80	80	65

Table II-A

75 cm^2 Air Electrode Construction

	Current Collector			Active Material			Process	Thickness
Electrode	Type	No.	Wt(gms)	Type	No.	Wt(gms)		(mils)
LU-021	Ni-Fiber	4	4.8	C-1,D-1,A-1	4	8.0	Preform	55
-022	Steel Wool	4	4.8	C-1,-2,D-1,A-1	4	8.5	Preform	62
-023	Steel Wool	4	4.1	C-1	4	8.0	Preform	64
-024	Steel Wool	4	4.9	C-1	4	8.0	Preform	74
-025	Steel Wool	4	5.0	C-1,C-2,D-2	4	7.5	Preform	68
-026	Steel Wool	6	4.8	C-2,D-2	6	6	Preform	49
-027	Steel Wool	4	5.0	DC-1	4	8	Preform	49
-028	Steel Wool	4	5.0	DC-2	4	8	Preform	53
-029	Steel Wool	4	7.6	DC-1	4	6.8	Acetone-paste	62
-030	Steel Wool	4	5.0	DC-2,-3,-4	4	10	Preform	59
-031	Steel Wool	4	5.0	DC-2,-3,-4		10	Preform	59
-032	Steel Wool	4	5.1	DC-3	4	8.5	Preform	49
-033	Steel Wool	4	5.1	DC-4	4	8.6	Preform	51
-034	Steel Wool	4	5.2	DC-5	4	9.5	Preform	71
-035	Ni-Fiber	8	5.2	C-4-E	4	16	Wet-Pasting	--

Table II-B

75 cm^2 Air Electrode Construction

	Current Collector			Active Materials				
Electrode	Type	No.	Wt(gms)	Type	No.	Wt(gms)	Process	Thickness (mils)
LU-036	Ni-Fiber	4	5.6	Same as cells#31,#32		7.5	Wet-pasting(rolled)	37
-037	Ni-Fiber	3	4.4	B-1,B-2		5.1	Wet-pasting	43
-038	Ni-Fiber	3	4.1	B-1,B-2		5.6	Wet-pasting	46
-039	Ni-Fiber	4	5.2	Same as Cell #68		9.4	Wet-pasting	58
-040	Ni-Fiber	4	5.5	A-2,E-1		8.9	Wet-pasting	71
-041	Ni-Fiber	4	5.5	A-2,E-2		8.8	Wet-pasting	66
-042	Ni-Fiber	4	5.5	A-2,E-3		8.9	Wet-pasting	71
-043	Ni-Fiber	4	5.5	A-2,E-4		9.1	Wet-pasting	70
-044	Ni-Fiber	4	5.5	A-2,E-5		9.5	Wet-pasting	72
-045	Ni-Fiber	2	2.1	A-2,E-2,F-1		2.5	Wet-pasting	44
-046	Ni-Fiber	3	4.6	G-1,G-2,G-3 (Fe pwd. added)		5.7	Wet-pasting	43
-047	Ni-Fiber	3	4.4	G-1,G-2,G-3		5.0	Wet-pasting	46
-048	Ni-Fiber	3	4.7	G-1,G-2,G-3 (Fe pwd. added)		5.7	Wet-pasting(rolled)	35
-049	Ni-Fiber	3	3.9	G-1,G-2,G-3		4.9	Wet-pasting(rolled)	38
-050	Ni-Fiber	3	4.4	G-1,G-2,G-3 (Fe pwd. added)		6.3	Preform	41
-051	Ni-Fiber	3	4.0	G-1,G-2,G-3 (Fe pwd. added)		6.4	Preform	40
-052	Ni-Fiber	2	2.7	G-1,G-2,G-3 (Fe pwd. added)		4.7	Preform	32
-053	Ni-Fiber	3	4.0	G-1,G-2,G-3 (Fe pwd. added)		6.4	Preform	41
-054	Ni-Fiber	2	2.8	G-1,G-2,G-3 (Fe pwd. added)		4.7	Preform	30
-055	Steel Wool	3	3.9	G-1,G-2,G-3 (Fe pwd. added)		7.5	Preform	63
-056	Steel Wool	2	2.6	G-1,G-2,G-3 (Fe pwd. added)		5.5	Preform	44

Table III-A

Discharge Potentials of Air Electrodes (mV vs Hg/HgO)
at Current Density of 25 mA/cm^2

Electrode	Cycles 3	27	51	75	99	123	147	171	195	219	243	Failure Mode @ Cycles
LU-015	-188	-147	-135	-142	-144	-130	-437	--	--			High Voltage @ 147
-016	-208	-180	-183	-201	-206	--	--					High Voltage @ 105
-017	-181	-165	-168	-169	-167	-231	--	--	--			High Voltage @ 135
-018	-240	-183	-169	-189	-187	--	--	--	--			High Voltage @ 111
-019	-191	-161	-156	-153	-155	-115	-281	--	--			High Voltage @ 147
-020	-199	-163	-157	-159	-173	--	--	--	--			High Voltage @ 105
-021	-146	-126	-165	-160	-184	--	--	--	--			High Voltage @ 105
-022	-246	-149	-145	-124	-139	-230	--	--	--			Delamination @ 141
-023	-225	-138	-132	-126	-143	-172	--	--	--			Delamination @ 141
-024	-217	-134	-128	-127	-130	-158	--	--	--			Delamination @ 144
-025	-276	-153	-150	-146	-157	-204	--	--	--			Leakage @ 141
-026	-259	-143	-137	-139	-147	--	--	--	--			Leakage @ 102
-027	-252	-147	-155	--	--	--	--	--	--			Leakage @ 63
-028	-201	-181	--	--	--	--	--	--	--			Leakage @ 36
-029	-241	-247	-228	-333	--	--	--	--	--			High Voltage @ 78
-030	-164	-194	-180	-179	-207	--	--	--	--			Leakage @ 105
-031	-179	-212	-200	-203	-195	-181	--	--	--			High Voltage @ 130
-032	-168	-238	-173	--	--	--	--	--	--			Leakage @ 54
-033	-242	-240	-198	-194	-202	-192	-187	-200	--			Terminated @190
-034	-120	-126	--	--	--	--	--	--	--			Leakage @ 46
-035	-149	-140	-135	-148	--	--	--	--	--			Terminated @ 78

Table III-B

Discharge Potentials of Air Electrode (mV vs Hg/HgO)
at Current Density of 25 mA/cm^2

Electrode	Cycles 3	27	51	75	99	123	Failure Mode @ Cycles
LU-036	-223	-185	-179	-187	--	--	Leakage @ 75
-037	-160	-122	-100	-133	--	--	Leakage @ 75
-038	-171	-124	-106	-123	-137	--	Leakage @ 99
-039	-245	-174	-195	-234	-200	--	OFF Test @ 108
-040	-236	-242	-188	-210	-347	--	
-041	-182	-165	-143	-180	-246	--	
-042	-264	-176	-152	-222	-240	--	
-043	-275	-209	-200	-192	-156	--	
-044	-281	-253	-281	-264	-220	--	
-045	-160	-133	-257	--	--	--	Leakage @ 57
-046	-218	-176	-167	ON TEST			
-047	-204	-166	-157	ON TEST			
-048	-222	-180	-285	--	--	--	Leakage @ 63
-049	-203	-177	--	--	--	--	Delamination @ 39
-050	-177	-159	--	--	--	--	Leakage @ 63
-051	-200	--	--	--	--	--	Delamination @ 27
-052	-215	-178	ON TEST				
-053	-211	-189	ON TEST				
-054	-209	-163	ON TEST				
-055	-164	ON TEST					
-056	-202	ON TEST					

Table III-C

Discharge Potentials of Air Electrodes (mV vs Hg/HgO)
at Current Density of 25 mA/cm^2

Electrode	Cycles 3	27	51	75	99	123	147	171	195	219	243	Failure Mode @ Cycles
LS-020	-186	-157	-156	-153	-155	-163	--	--	--	--	--	Leakage @ 129
-021	-183	-143	-163	-142	-142	-179	--	--	--	--	--	High Voltage @ 138
-022	-184	-134	-148	-132	-128	-257	--	--	--	--	--	High Voltage @ 123
-023	-165	-129	-135	-131	-106	-286	--	--	--	--	--	High Voltage @ 123
-024	-213	-155	-153	-147	-148	-151	-155	-159	-160	-151	-151	Delaminated @ 249

Table IV-A

Charge Potentials of Air Electrodes (mV vs Hg/HgO)

at Current Density of 15 mA/cm^2*

Cycles

Electrode	3	27	51	75	99	123	147	171	195	219	243
LU-015	+610	+591	+643	+568	+595	+644	+616	--	--	--	--
-016	+651	+691	+793	+699	+788	--	--	--	--	--	--
-017	+712	+620	+673	+635	+639	+995	--	--	--	--	--
-018	+712	+626	+628	+634	+624	--	--	--	--	--	--
-019	+699	+619	+641	+630	+618	+677	+945	--	--	--	--
-020	+672	+615	+640	+713	+964	--	--	--	--	--	--
-021	+610	+598	+597	+603	+628	--	--	--	--	--	--
-022	+538	+525	+552	+690	+729	+939	--	--	--	--	--
-023	+595	+569	+590	+698	+746	+938	--	--	--	--	--
-024	+568	+568	+588	+651	+719	+961	--	--	--	--	--
-025	+576	+537	+559	+732	+784	+1,052	--	--	--	--	--
-026	+547	+532	+550	+616	+610	--	--	--	--	--	--
-027	+602	+600	+689	--	--	--	--	--	--	--	--
-028	+536	+542	--	--	--	--	--	--	--	--	--
-029	+550	+574	+576	+603	--	--	--	--	--	--	--
-030	+608	+615	+626	+780	+981	--	--	--	--	--	--
-031	+607	+600	+582	+619	+691	+902	--	--	--	--	--
-032	+601	+554	+701	--	--	--	--	--	--	--	--
-033	+630	+601	+664	+659	+738	+737	+781	+737	--	--	--
-034	+575	+573	--	--	--	--	--	--	--	--	--
-035	+550	+553	+557	+649	--	--	--	--	--	--	--

*Current density of 25 mA/cm^2 was used in LU-015 to LU-020 up to 86 cycles.

Table IV-B

Charge Potentials of Air Electrodes (mV vs Hg/HgO)
at Current Density of 25 mA/cm^2

Electrode	3	27	51	75	99	123
LU-036	+ 688	+765	+ 643	+ 636	--	--
-037	+ 599	+601	+ 677	+ 669	--	--
-038	+ 639	+643	+ 791	+ 743	+781	--
-039	+ 576	+575	+ 588	+ 624	+657	--
-040	+ 897	+831	+ 834	+ 651	+960	--
-041	+ 783	+624	+ 762	+ 779	+817	--
-042	+ 886	+651	+ 667	+ 886	+791	--
-043	+1,076	+720	+1,063	+1,025	+607	--
-044	+1,111	+983	+1,194	+ 934	+932	--
-045	+ 648	+617	+ 683	--	--	--
-046	+ 559	+553	+ 565	--------- O N T E S T ------		
-047	+ 605	+634	+ 679	--------- O N T E S T ------		
-048	+ 542	+546	+ 583	--	--	--
-049	+ 604	+615	--	--	--	--
-050	+ 538	+547	+563	--	--	--
-051	+ 536	--	--	--	--	--
-052	+ 573	+621	---------- O N T E S T ------			
-053	+ 542	+546	---------- O N T E S T ------			
-054	+ 563	+591	---------- O N T E S T ------			
-055	+ 516	---------- O N T E S T ------				
-056	+ 570	---------- O N T E S T ------				

Table IV-C

Charge Potentials of Air Electrodes (mV vs Hg/HgO)
at Current Density of 25 mA/cm^2

	Cycles										
Electrode	3	27	51	75	99	123	147	171	195	219	243
LS-020	+724	+631	+651	+620	+613	+960	--	--	--	--	--
-021	+701	+636	+623	+622	+726	+982	--	--	--	--	--
-022	+723	+638	+620	+619	+775	+809	--	--	--	--	--
-023	+695	+654	+631	+638	+1,014	+718	--	--	--	--	--
-024	+590	+601	+581	+572	+597	+611	+552	+578	+590	+686	+716

Table V-A

100 cm^2 Air Electrode Active Material

Compositions of Air Electrode Active Material

	A	B	C	D	E	F	G	H	I	J	K	L
Shawinigan Black	9	9	9	9	12	12	12	12	9	9	9	9
FEP	3	3.3	3.6	3.9	4	4.4	4.8	5.0	3.3	3.6	3.9	3.9
Teflon 30B	3.5	3.1	2.7	2.4	5	4.5	4	3.5	3	2.7	2.4	2.1
WC-12 w/o Co	3	3	3	--	2.4	2.4	2.4	--	3	3	3	--
$AgNO_3$	3	3	3	--	4	4	4	--	3	3	3	--
$FeWO_4$	--	--	--	--	2.4	2.4	2.4	--	--	--	--	--
NiS	--	--	--	--	2.4	2.4	2.4	--	--	--	--	--
*0.2% FC-95	--	--	--	--	--	--	--	--	60	35	20	--
H_2O	59	59	59	59	60	60	60	55	--	25	40	50
Cell Identifications	Cells #31-39 & Cells #54-56 (Ni powder is used instead of WC-12 w/o Co in Cells #54-56)				Cells #40-42 & Cells #63-68				Cell #43			

* Fluorochemical surfactant by 3M Company

Table V-B

100 cm^2 Air Electrode Active Material

	Compositions of Air Electrode Active Material										
	E'	F'	G'	H'	M	N	O	P	Q	R	S
Shawinigan Black	12	12	12	12	9	9	9	9	9	9	9
FEP	4.2	4.8	5.2	5.5	3.1	3.3	3.6	3.9	3.3	3.6	3.9
Teflon 30B	4.8	4.5	4.0	3.5	3.3	3.0	2.7	2.4	--	--	--
Teflon 6	--	--	--	--	--	--	--	--	1.5	1.7	2
WC-12 w/o Co	2.4	2.4	2.4	--	--	--	--	--	3	3	--
$AgNO_3$	4	4	4	--	--	--	--	--	3	3	--
$FeWO_4$	2.4	2.4	2.4	--	--	--	--	--	--	--	--
NiS	2.4	2.4	2.4	--	--	--	--	--	--	--	--
0.2% FC-95 (ml)	60	40	20	--	--	--	--	--	--	--	--
H_2O (ml)	--	20	40	55	65	65	60	60	60	60	60
	Cells #44 - 46				Cells #47 - 49				Cell #50		

Table V-C

100 cm^2 Air Electrode Active Material

	Compositions of Air Electrode Active Material									
	T	U	V	W	T'	U'	V'	W'	X	Y
Shawinigan Black	9	9	9	9	9	9	9	9	10	5
FEP	3.3	3.5	3.7	3.9	3.3	3.5	3.7	3.9	3	1.5
Teflon 30B	--	--	--	--	--	--	--	--	3	1.5
Teflon 6	2	2	2.2	2.2	2	2	2.1	2.3	--	--
WC-12 w/o Co	3	3	3	--	--	--	--	--	--	10
$AgNO_3$	3	3	3	--	--	--	--	--	--	5
Ni (325 mesh)	--	--	--	--	--	--	--	--	4	--
*Dil. Triton X-100 (ml)	65	60	50	25	65	60	50	25	--	50
H_2O	--	--	10	35	--	5	15	35	60	--
	Cells #51 and Cell #53 (lower Teflon 6 content in Cell #53)				Cell #52				Cells #57-58	

* A 1.7 g Triton X-100/500 ml H_2O

Table V-D

100 cm^2 Air Electrode Active Material

	Compositions of Air Electrode Active Material										
	AA	BB	CC	DD	EE	FF	GG	HH	II	JJ	KK
Shawinigan Black	6.5	6.5	6.5	6.5	6.5	6.5	10	12	12	12	12
Ketjen Black	3.5	3.5	3.5	3.5	3.5	3.5	--	--	--	--	--
FEP	3.5	3.8	4.1	1.5	1.8	2.0	2.0	2.0	2.5	2.5	2.0
Teflon 30B	3.5	3.1	2.7	3.0	2.5	2.5	2.5	2.5	2.5	2.5	2.0
WC-12 w/o Co	3.3	3.3	3.3	3.3	3.3	3.3	3.3	4.0	4.0	4.0	--
$AgNO_3$	3.3	3.3	3.3	3.0	3.0	3.0	3.0	4.0	4.0	4.0	--
NiS	--	--	--	--	--	--	--	3.0	3.0	3.0	--
*Dil. Triton X-100 (ml)	--	--	--	10	10	5	--	30	20	10	--
H_2O (ml)	66	66	66	55	55	65	65	55	60	65	70
Cell Identification	Cells #59 - 62			Cells #69 - 73				Cells #74 - 75			

* A 1.7 g of Triton X-100/500 ml H_2O

Table VI-A

Pasting Specifications of Active Material on Various Air Electrode Layers

Plaque Number (Electrolyte side) ↑		Cells (#31,#32)	(#33,#34)	(#35,#36)	(#37,#38,#39)	(#40,#41,#42)	(#43)
1.	-a	*A (6)	A (9)	A (9)	A (11)	E (6)	I (9)
	-b	A (6)	A (6)	A (6)	A (6)	E (6)	I (6)
2.	-a	B (6)	B (9)	B (9)	A (11)	E (9)	I (10)
	-b	B (6)	B (6)	B (6)	B (6)	F (6)	J (6)
3.	-a	B (6)	B (9)	B (9)	B (11)	F (9)	J (10)
	-b	C (6)	C (6)	B (6)	B (6)	F (6)	J (6)
4.	-a	C (6)	C (9)	C (9)	C (11)	G (9)	K (10)
	-b	D (6)	‡ (5)	‡ (4)	D (6)	H (6)	L (6)

(Air side)

* Y(X) denotes X grams of the active material with composition Y were pasted on that side of the current collector.

‡ Preform of carbon, FEP and Teflon 30B by dry powder method.

Table VI-B

Pasting Specifications of Active Material on Various Air Electrode Layers

Plaque Number (Electrolyte side)		Cells (#44,#45,#46)	(#47,#48)	(#49)	(#50)	(#51,#53)	(#52)	(#54,#55,#56)
1.	-a	E'(9)	M(9)	M(8)	Q(9)	T(9)	T'(9)	A(9)
	-b	E'(6)	M(6)	--	Q(6)	T(6)	T'(6)	A(6)
2.	-a	E'(9)	M(9)	M(8)	Q(9)	T(9)	T'(9)	B(9)
	-b	F'(6)	N(6)	--	Q(6)	T(6)	T'(6)	B(6)
3.	-a	F'(9)	N(9)	M(8)	Q(9)	U(9)	U'(9)	B(9)
	-b	F'(6)	N(6)	--	R(6)	U(6)	U'(6)	B(6)
4.	-a	G'(9)	O(9)	N(8)	R(9)	V(9)	V'(9)	C(9)
	-b	H'(6)	P(6)	--	S(6)	W(6)	W'(6)	D(9)
5.	-a	--	--	N(8)	--	--	--	--
	-b	--	--	--	--	--	--	--
6.	-a.	--	--	O(8)	--	--	--	--
	-b.	--	--	P(8)	--	--	--	--

(Air side)

Lighter Ni-fiber current collectors were used in Cell #49.

Table VI-C

Pasting Specifications of Active Material on Various Air Electrode Layers

Plaque Number (Electrolyte side)		Cells (#57,#58)	(#59,#60,#61,#62)	(#63,#64,#65, #66,#67,#68)	(#69,#70,#71, #72,#73)	(#74,#75)
1.	-a	X(9)	AA(9)	E(9)	DD(9)	HH(4,5)
	-b	X(6)	AA(6)	E(6)	DD(6)	HH(6)
2.	-a	X(9)	BB(9)	E(9)	EE(9)	II(9)
	-b	X(6)	BB(6)	F(6)	EE(6)	II(6)
3.	-a	X(9)	BB(9)	F(9)	EE(9)	JJ(9)
	-b	X(6)	BB(6)	F(6)	FF(6)	KK(4)
4.	-a	X(9)	CC(9)	G(9)	GG(9)	--
	-b	X(6)	D (6)	H(6)	GG'(3)	--

(Air side)

In Cells #57 and #58, wet Y material was pasted into the cracked zones of each plaque.

Cells #63, #64, #67 were assembled into 3 cell batteries.

GG': dry powder; same composition as GG without WC-12 w/o Co and $AgNO_3$.

Dwg. 6424A10

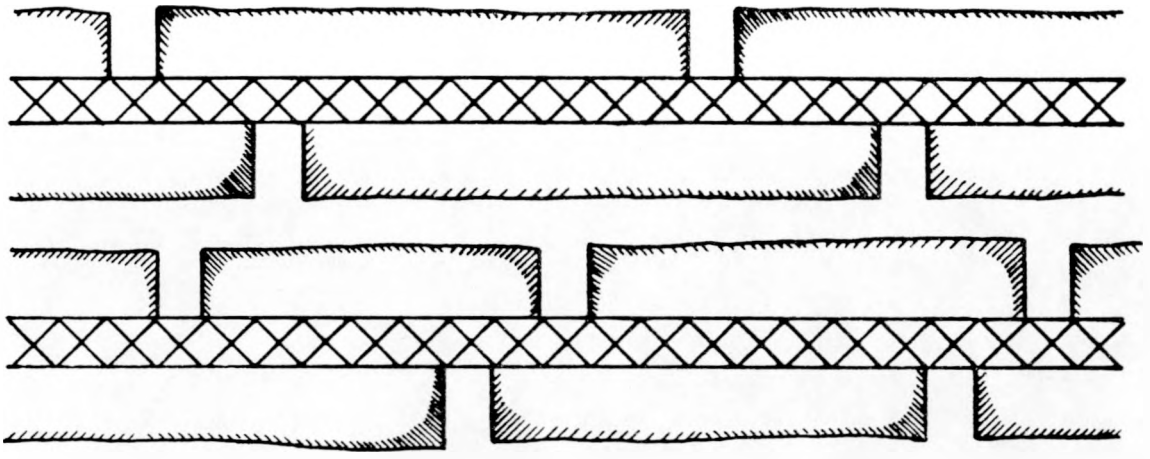

Before Pressing

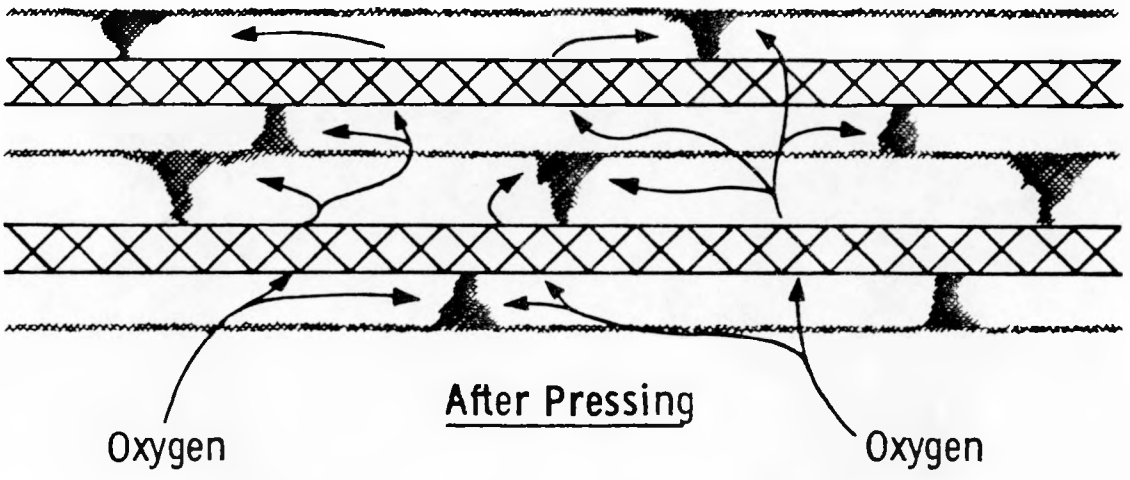

Fig. 1—Concept of bifunctional air electrode prepared by wet pasting technique

IV. IRON ELECTRODE STUDIES

4.1 INTRODUCTION

Work Period Goals

For the period covered by this report (June 1977-June 1978) the foremost goal was to determine the processing parameters for the fabrication of iron electrodes that could consistently yield discharge capacities of 0.4 A hr/gm and greater at a current density of 50 mA/cm^2. It was further desired that this discharge capacity be achieved at a voltage of -0.9 V. (Hg/HgO reference) or lower and that the electrode be about 25 to 30 percent dense (based on the theoretical density of iron) and about 0.100 inches in thickness.

General Description of Work Plan

In the previous contract period (June 1976-June 1977) a start was made in the direction of improving the discharge capacity of iron electrode prepared by powder metallurgy techniques. Various properties of the sponge iron powder and its Fe_2O_3 parent material were measured and correlated. The conclusion was reached that discharge capacity was most influenced by the pore size (or roughness of texture) of the iron powder particles rather than by the total surface area of the particles, per se. In other words, it is only the total electrode surface area which is accessible to electrolyte that is important to the performance of the iron electrode. Furthermore, as shown by the results of the previous annual report,[1] this area must be accessible for more than a single charge-discharge cycle.

Several approaches to increasing total surface area were considered in the current work period. More generally, these were treatments intended to increase the capacity of the iron electrode whether by increasing surface area, altering the defect structure of the iron or other. [No direct measurements of these parameters were made. The only measure of success or failure of an "activation" treatment was the change in discharge capacity which it effected.] The activation treatments included lowering the temperature of Fe_2O_3 reduction, using smaller iron particles and oxidizing-reducing the iron particles.

To increase electrolyte accessibility, the work on spacer (pore former)materials was continued. Other means of increasing discharge capacity were to optimize electrode density (discussed further in the following section, electrode thickness and the design of the electrode current collector.

Physical Model of an Iron Electrode

For an iron electrode to function at high discharge capacity, it must possess extensive total surface area, pores of sufficient size and number, and low resistance provided by considerable inter-particle bonding. Extensive surface area is essential since the electrochemical reactions which accompany charge and discharge occur at the iron-electrolyte interface. However, the second condition must also be satisfied to assure superior electrode discharge capacity. The physical structure (pore size and number) of the electrode must be such that electrolyte is readily accessible to all portions of the electrode. Accessibility is favored by a high degree of porosity with the pores being neither too small to hold sufficient electrolyte for optimum extent of reaction nor too large to produce an accompanying critical decrease in surface area. The third condition requires no further explanation. In order to gain additional insight into the second of these structural features, a simple model based on the work of Selanger[2] was formulated.

These structural conditions are represented, respectively, by the pores labeled "insufficient porosity" and "excessive porosity" in Figure 4-1. It is assumed that there is no capacity limitation due to insufficient surface area or weak interparticle bonds. In this representation of an iron electrode the total initial porosity of the electrode is contained within a single pore. For the condition of insufficient initial porosity, the pore is completely filled with $Fe(OH)_2$ discharge product before all the iron associated with the pore can react. At the other extreme, excessive initial porosity results in all the iron reacting to form $Fe(OH)_2$. However, the relatively low ratio of iron volume to pore volume results in a certain portion of the void being retained

Dwg. 6439A02

SCHEMATIC REPRESENTATION OF IRON ELECTRODE FOLLOWING UPPER PLATEAU DISCHARGE

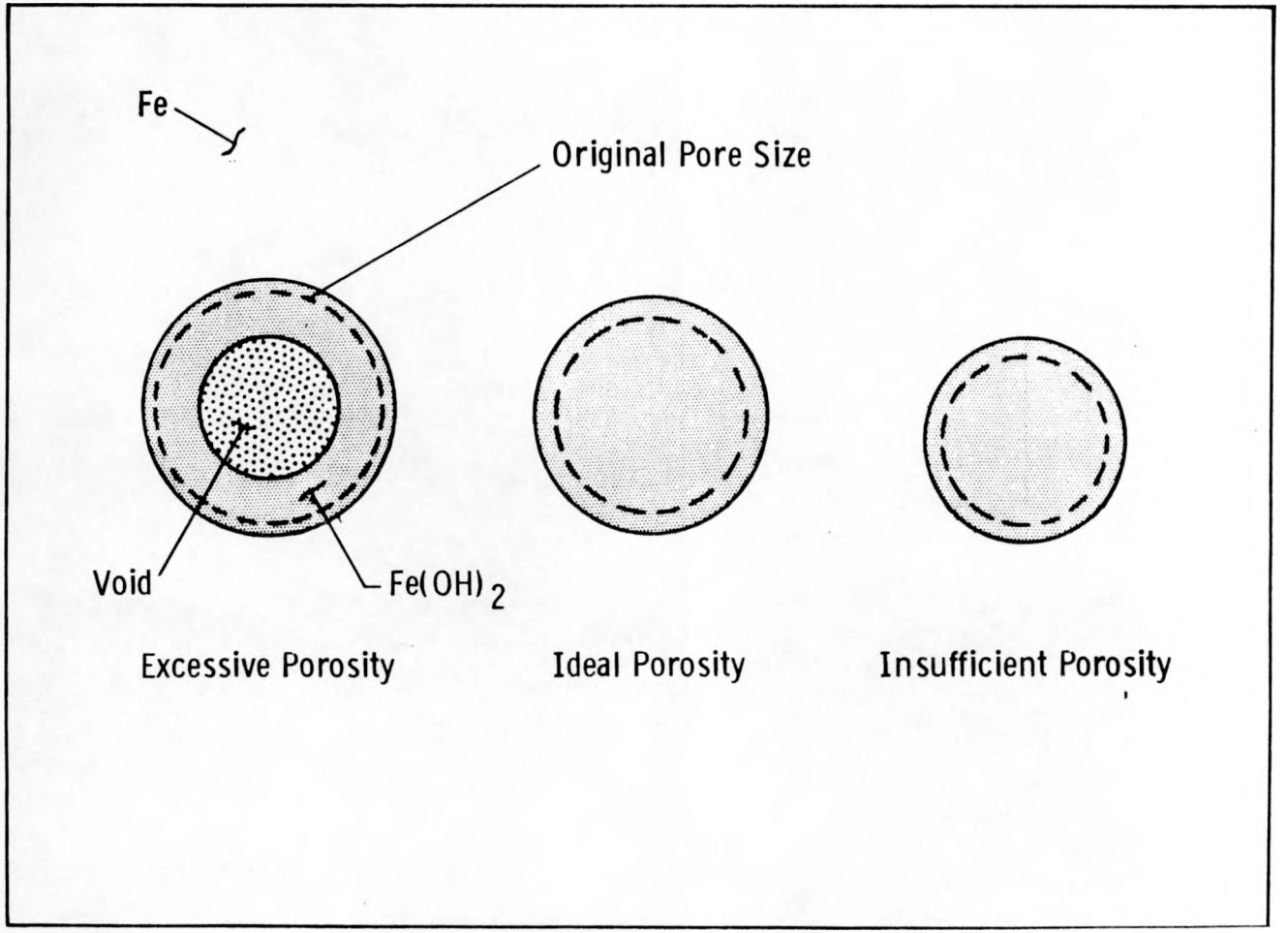

Figure 4-1: Schematic Representation of an Iron Electrode Following Upper Plateau Discharge

at the completion of upper plateau discharge. In the case of the ideal amount of porosity, the initial pore volume is just sufficient to contain the $Fe(OH)_2$ formed when all the iron has reacted.

Details of the model are given in the Appendix. The results of model calculations are shown in Figures 4-2 and 4-3. In the former, maximum discharge capacity in A·hr/unit volume is presented as a function of the electrode's initial porosity (100% minus the density on a percent of theoretical density of iron basis, % TD_{Fe}). It is indicated that the optimum percentage of initial porosity should be about 75 to 80%, i.e., for an electrode of 20 to 25% TD_{Fe}, theoretically all the iron can be transformed to $Fe(OH)_2$. The maximum discharge capacity expressed on an active weight basis (Figure 4-3) is the greatest for electrodes of 25% TD_{Fe} and less. [The theoretical, upper plateau discharge capacity of 0.962 A·hr/gm is not approached since the model has assumed that a small percentage (about 5%) of the active material volume has been replaced by the current collector.]

Two purposes were served by the model. A target electrode density was established, but remained to be verified experimentally. Also, by providing a measure of maximum possible discharge capacity theoretically obtainable under the optimum combination of cell operation parameters and other structural features of the electrode, a scale is provided against which we can gauge our performance in developing a high capacity iron electrode.

Curve 696639-A

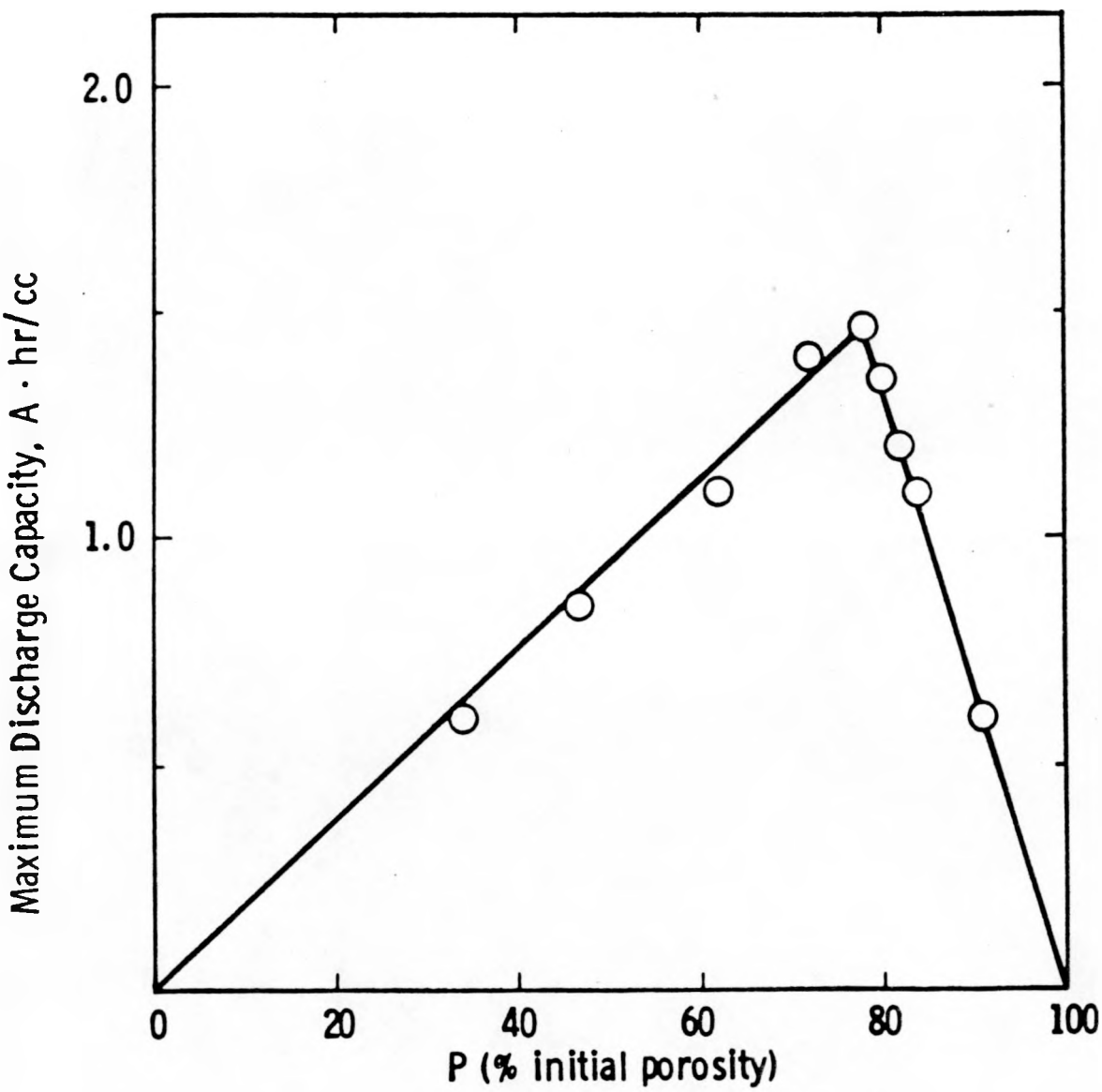

Figure 4-2: Model Calculations of Maximum Discharge Capacity (Volume Basis).

Curve 696640-A

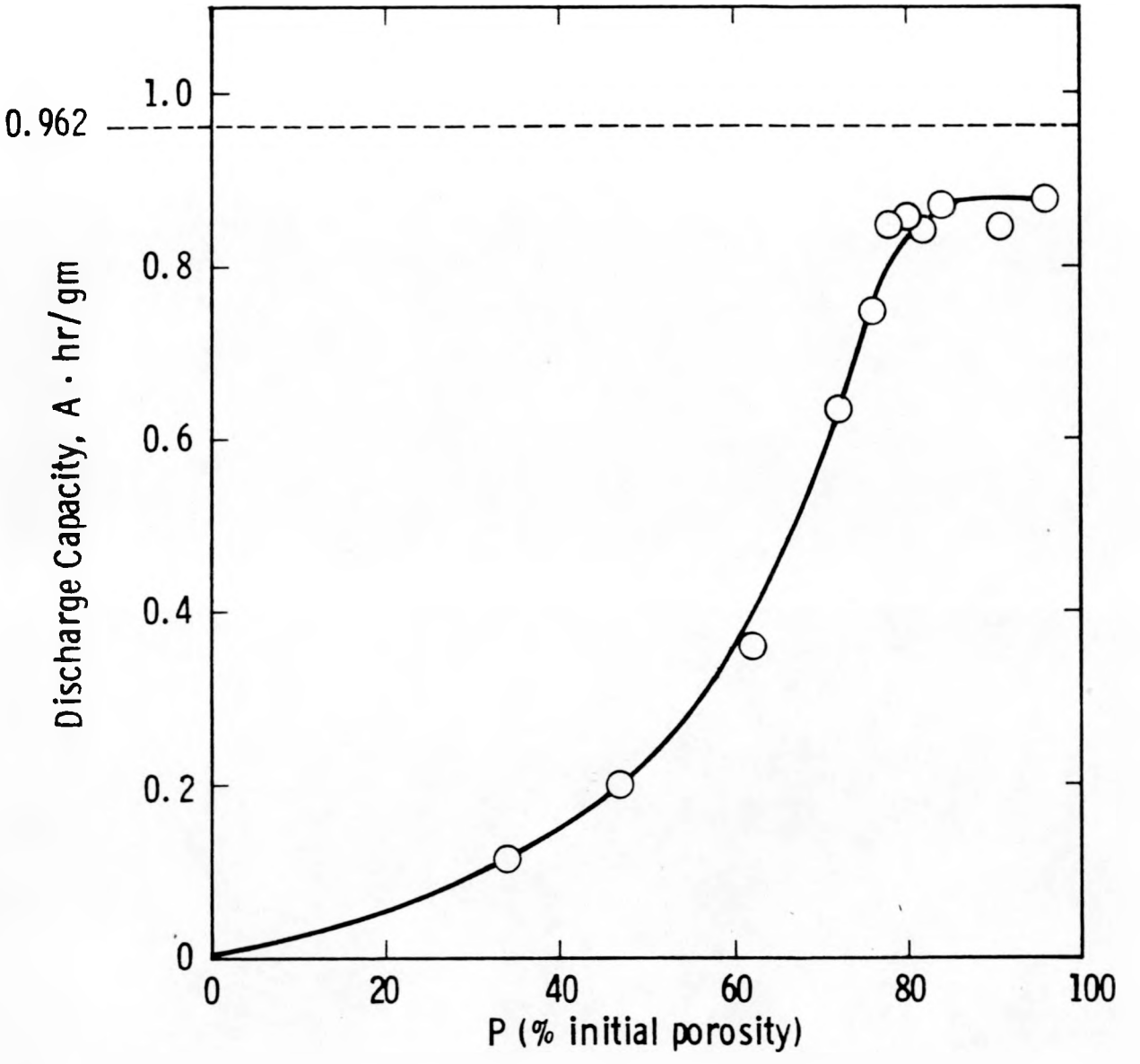

Figure 4-3: Model Calculations of Maximum Discharge Capacity (Weight Basis)

4.2 PROCEDURE

Iron powder was prepared by the hydrogen reduction of Fe_2O_3 for about one hour at temperatures between 680°C and 750°C. Screening to remove any particles greater than 20 mesh followed. Other powder operations, such as oxidation-reduction, further screening or spacer (pore former) additions, were often employed. These operations are fully described in appropriate sub-sections of Experimental Results (Section 4.3).

Small (10 cm^2) electrodes were prepared from iron powder by powder metallurgy techniques. Pressing utilized a 1.25 inch square steel die and a pressure range from 1280 psi to about 5000 psi. During the pressing operation perforated nickel sheet was incorporated into each major face of the electrode to serve both as a sinter shrinkage retardant and, for the great majority of electrodes, as a current collector. In some electrodes, either fiber (nickel, steel) or nickel performated sheet was added to the interior of the electrode during the pressing sequence. Hydrogen sintering was accomplished in a moving belt furnace. Temperatures between 650°C and 900°C and times (at temperatures) between 4 and 240 minutes were employed. Following sintering, determinations were made of weight loss, shrinkage in the thickness direction and density change. Prior to half-cell testing, sintered electrodes were provided with nickel current collector tabs.

Half-cell testing of iron electrodes utilized a nickel dummy electrode and a Hg/HgO standard reference. Temperature stability was provided by immersion of the acrylic half-cell cases in a stirred water bath. Charge and discharge current densities (100 mA/cm^2 and 50 mA/cm^2 unless otherwise stated), upper plateau discharge cutoff voltage (0.750 V) and cycle times were controlled automatically. A very large excess of electrolyte (20 cc per gram of iron of 25% KOH) was generally used because of the simplification to the experimentation which it provided. Water was added to the half-cells at completion of the 7th and 20th cycles to maintain the starting KOH concentration.

4.3 EXPERIMENTAL RESULTS

4.3.1 Fe_2O_3 Powder Studies

Work was extended from the previous contract period on the evaluation of Fe_2O_3 powders. The aim was to characterize vendor-supplied Fe_2O_3 according to those powder properties which had been found to influence electrode discharge capacity. Nominally 25% theoretical density electrodes were prepared from unscreened, untreated powder. No pore forming agent was used. Following sintering for 10 minutes at 900°C, electrodes prepared from a number of Fe_2O_3 powder lots were half-cell tested at 40°C in 25 wt. percent KOH. From these results (Figure 4-4) sinter shrinkage (previously adopted as the measure of iron particle texture or roughness) was confirmed to correlate with discharge capacity. Iron powder particles possessing a relatively open structure are superior to smoother particles even though their total surface areas might be equal. [A more complete discussion of this point is contained in Section 4.2.1.1 of Ref. 1.]

Further support was gathered for the contention that electrode sinter shrinkage (particle roughness) was influenced by the sulfur content of the parent Fe_2O_3 (Figure 4-5). An even better correlation was obtained between sinter shrinkage (particle roughness) and the product of the sulfur content and the B.E.T. surface area of the parent Fe_2O_3 (Figure 4-6). Apparently the sintering rate of the ultrafine, freshly reduced iron particles into larger iron particles (agglomerates) during the reduction operation is sufficiently enhanced by both the increased Fe_2O_3 surface area and Fe_2O_3 sulfur content that increased product water vapor entrapment produces a more rough-textured (larger pore) iron powder. This condition of overfiring of Fe_2O_3 due to the presence of sulfur (which accompanies its reduction to metallic iron) has been discussed in the literature[3].

As a result of the correlation found in Figure 4-6, an attempt was made to buy the best Fe_2O_3 commercially available based on a specification for sulfur content and B.E.T. nitrogen adsorption surface area. However all vendors contacted declined to quote on this basis. Work in the area

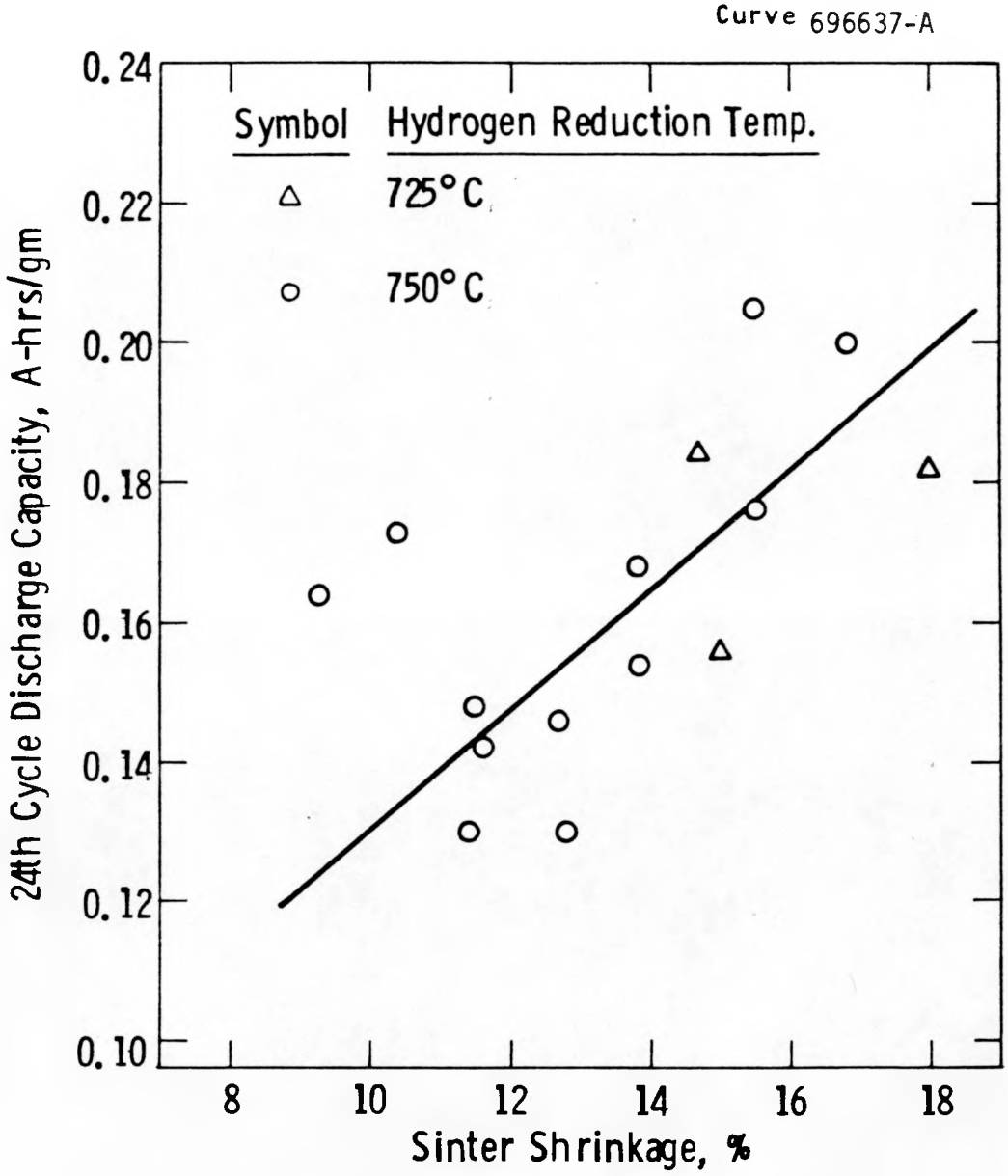

Figure 4-4: The Dependence of Iron Electrode Discharge Capacity on Iron Powder Texture (as Measured by Sinter Shrinkage).

Curve 692957-A

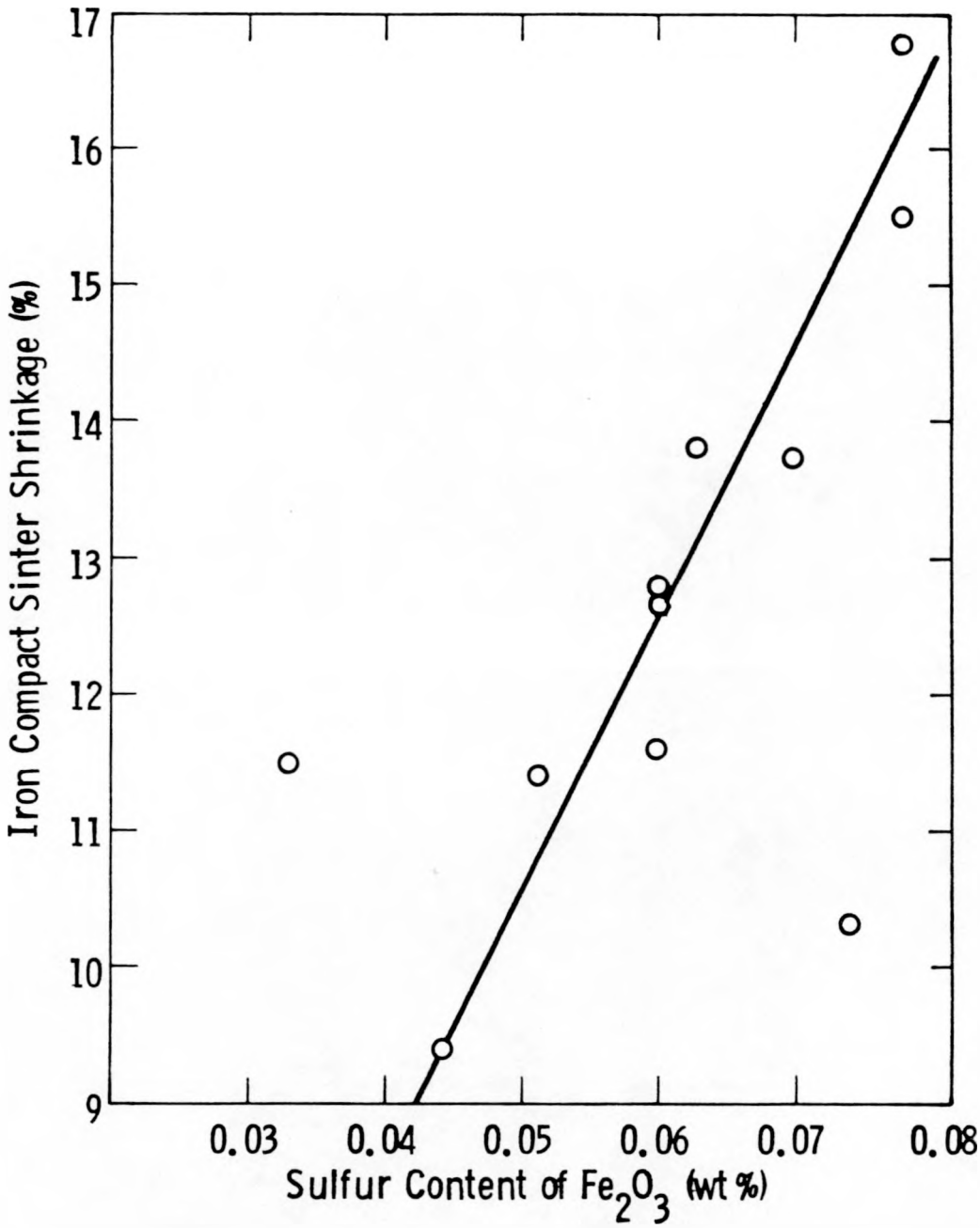

Figure 4-5: Iron Particle Texture (as Measured by Sinter Shrinkage) Dependence on Fe_2O_3 Sulfur Content. (Data are limited to Iron Powders formed by 750°C Hydrogen Reduction).

Curve 692958-A

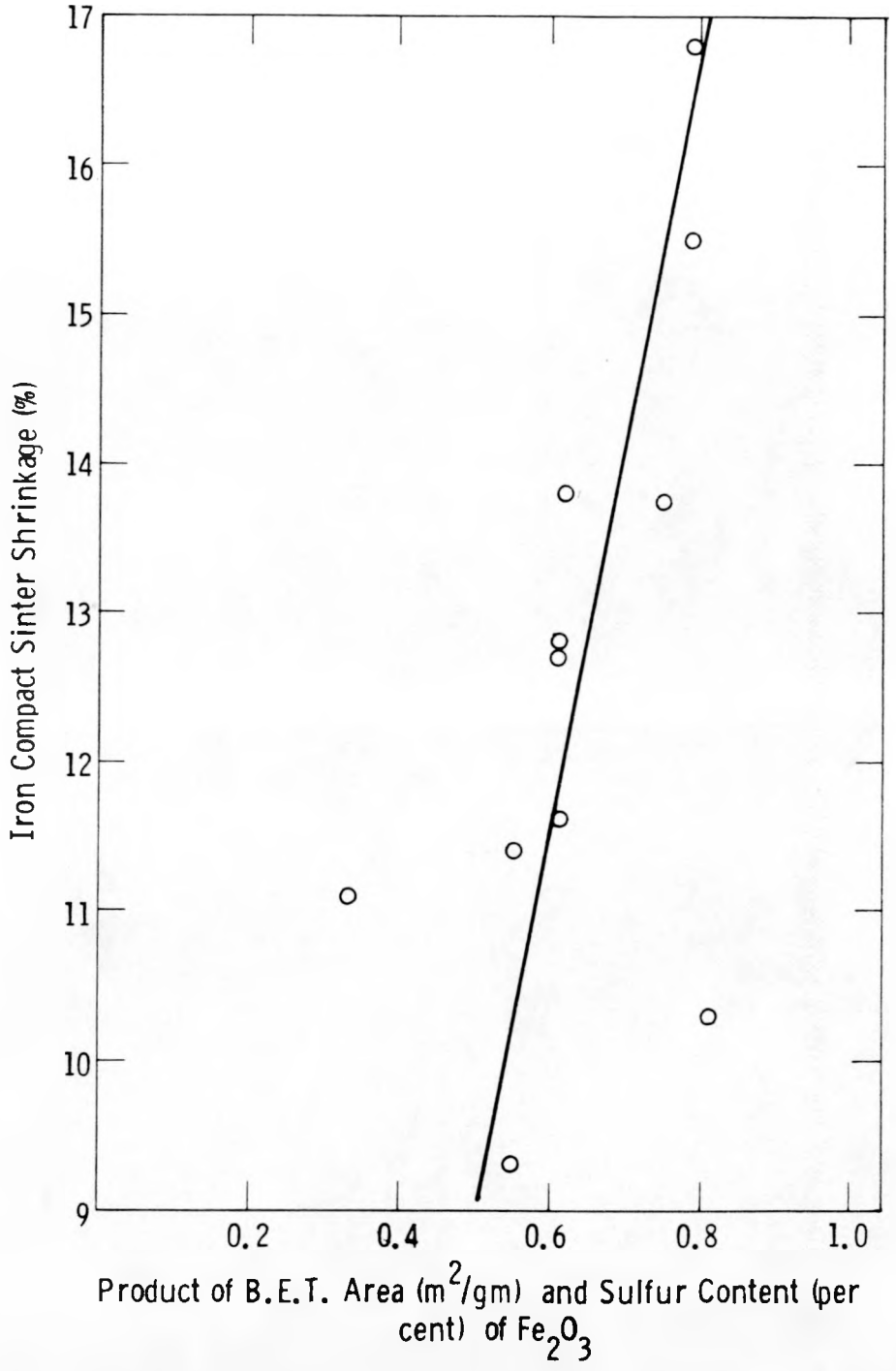

Figure 4-6: Iron Particle Texture (as Measured by Sinter Shrinkage) Dependence on Fe_2O_3 Properties. (Data are limited to Iron Powders formed by 750°C Hydrogen Reduction,)

of Fe_2O_3 powder evaluation was sidelined in favor of a more concentrated effort to increase the activity of iron powder, and with it, the discharge capacity of iron electrodes.

4.3.2 Fe Powder Activation Studies

Fe Powder Activation

Based on the results of the Fe_2O_3 powder evaluation, lot number 4 Fe_2O_3 (Fisher Scientific Co. lot number 763335) was selected for use in this phase of the program. Previous use of this powder lot produced electrode discharge capacities that were approximately mid-range for all lots evaluated. The use of other powder lots is indicated where appropriate.

Three means of increasing the "activity" of iron powder were evaluated. These included:

1. Further work on the influence of particle size on electrode discharge capacity. This operation is one of particle sizing and is designated S in several of the data Figures which follow.
2. An evaluation of various chemical treatments applied to the iron powder. This operation is designated by the letter T.
3. An evaluation of Fe_2O_3 reduction temperature (designated by the letter R).

The criterion employed was the 20th cycle discharge capacity obtained on 10 cm^2 electrodes having a sintered density within the range of 20 to 25% TD_{Fe}. For a number of electrodes, urea pore forming material (spacer) was added to the iron powder prior to pressing in order to prevent excessive shrinkage during sintering which would, if permitted, limit the extent of accessibility of electrolyte to the inner regions of the electrode. The choice of 10 volume percent urea of a 115 micron nominal particle size (-170, +100 mesh) was substantiated later in the program, as was the choice of sintering parameters of 10 minutes at 800°C. These results are presented in a later portion of this section (4.3.2).

The results of preliminary iron-air battery design studies suggested that optimum iron electrode density and thickness should be in the neighborhood of 25 percent of the theoretical density of iron (25% TD_{Fe}) and 0.100 inch respectively. Thus these values were adopted for the electrodes prepared for the studies on iron power activation. Half-cell testing utilized 25 weight % KOH containing 15 gm/l LiOH and a cell temperature of 44°C. Other parameters included 100 mA/cm^2 charge and 50 mA/cm^2 discharge to a cutoff of 0.750 volts.

The relation between discharge capacity and iron particle size is given by Figure 4-7. Lot 0 Fe_2O_3 powder (Fisher Scientific Company lot number 743290) was used throughout in this series of experiments since the electrodes prepared from the larger particles had already been tested well before the beginning of the latest contract period. For the two smallest particle sizes (nominally 18 and 42 microns) urea particles were added to the iron powder since, without them, densification during sintering would have been excessive. A significant increase in discharge capacity was realized for electrodes prepared from these smallest iron particles. The iron particle sizing operation (S) was thus established to consist of screening to discard all but the nominal 18 micron, (<400 mesh) particles. When this operation was applied to lot 4 iron powder, a discharge capacity of 0.24 A·hr/gm was realized. This is a significant improvement upon earlier results (compare entries 1 and 2 of the Progress Summary chart of Figure 4-8). A comparable improvement in discharge capacity was found for electrodes prepared from lot 0 powder as evidenced by a comparison of the same two entries.

The addition of small amounts of several metal sulfates to the iron powder was evaluated as to the effect on electrode discharge capacity. Additions were made by mixing a slurry of iron powder, metal sulfate and distilled water for 4 hours (or longer), drying in air to a cake at 65°C-80°C and comminuting by forcing the dried cake through a 60 mesh screen. The half-cell results are given in Figure 4-9. Here the type and amount of additive are also presented, the numerals referring

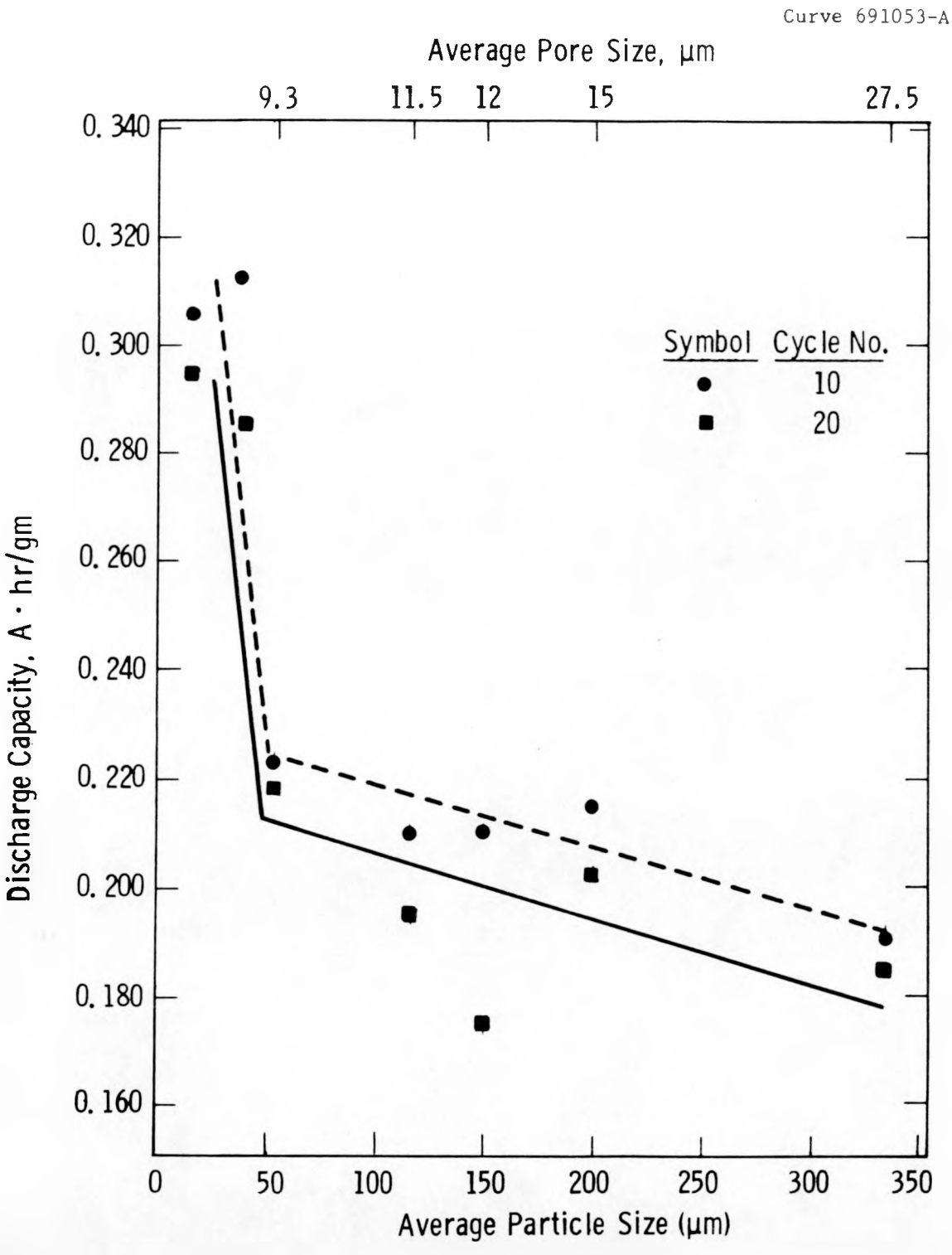

Figure 4-7: The Influence of Particle Size on Iron Electrode Discharge Capacity

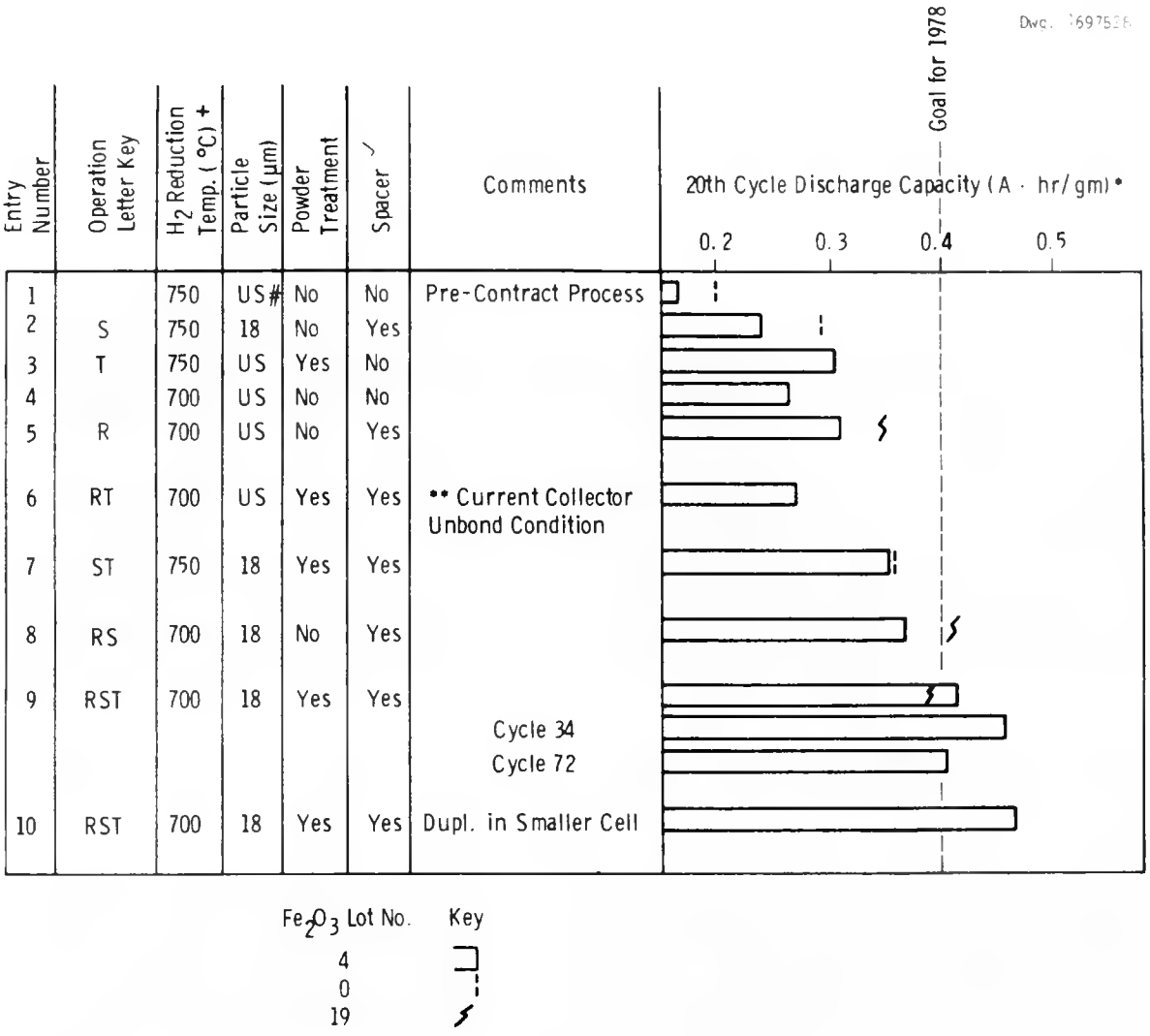

* 44°C, 25 Wt. % KOH with 15 Gram/Liter LiOH, 50 mA/cm^2 Discharge to 0.750 Volts, 100 mA/cm^2 Charge

++ Unscreened

\+ All Sintering at 800°C for 10 Minutes

⌣ 115 Micron (Nominal) Urea In the Amount of 10 Vol. %

** Perforated and Expanded Nickel Metal Sheet Used as Current Collector

Figure 4-8: Progress Summary Chart for Iron Powder Studies

Figure 4-9: Discharge Capacity of Electrodes Prepared from Iron Powders Given Various Oxidation Treatments.

to weight percent relative to iron and the chemical symbols Mg, Cd, Cr referring to the respective compounds $MgSO_4$, $CdSO_4 \cdot 8\ H_2O$ and $CrSO_4 \cdot n\ H_2O$. All but one of the powder treatments (the addition of 2 wt.% $CrSO_4 \cdot n\ H_2O$) resulted in increased discharge capacity, while many of the treatments produced a very marked increase in discharge capacity over that realized with the pre-contract electrode preparation process (identified as "untreated" in Figure 4-9). The treatment chosen for further application was the addition of 2.4 wt.% $CdSO_4 \cdot 8\ H_2O$. With the substitution of 800°C sintering for 900°C sintering the chemical treatment operation (T) was established (entry number 3 of the Progress Summary Chart, Figure 4-8).

The final means studied for increasing the "activity" of iron powder was a decrease in the temperature of Fe_2O_3 reduction from 750°C to temperatures as low as 690°C for lot 4 powder. The 20th cycle half-cell discharge capacity data for this series of experiments are given in Fig. 4-10. A reduction temperature of 700°C was chosen as optimum. Since the 700°C reduced powder containing urea spacer was found to produce superior electrode discharge capacity compared to the same powder without spacer, the former variant was adopted as the reduction operation (R). Both variants are, however, included in the Progress Summary Chart (Figure 4-8), as entries 5 and 4 respectively, where they can be compared to entry 1 for the pre-contract process. With the substitution of lot 19 Fe_2O_3 powder for the lot 4 Fe_2O_3 powder, the incorporation of the new reduction operation (R) produced an electrode discharge capacity of 0.35 A•hr/gm.

In the next stage of the work, the iron powder "activation" operations were evaluated in pairs, i.e., RT, ST, and RS. The 20th cycle discharge capacities for electrodes made by these processes are given in entries 6, 7 and 8 of the Progress Summary Chart (Figure 4-8). Hydrogen reduction at 700°C coupled with iron powder treatment with $CdSO_4 \cdot 8\ H_2O$ (RT) did not improve discharge capacity beyond the average result obtained with the single powder activation treatment (T). In addition,

Curve 695734-A

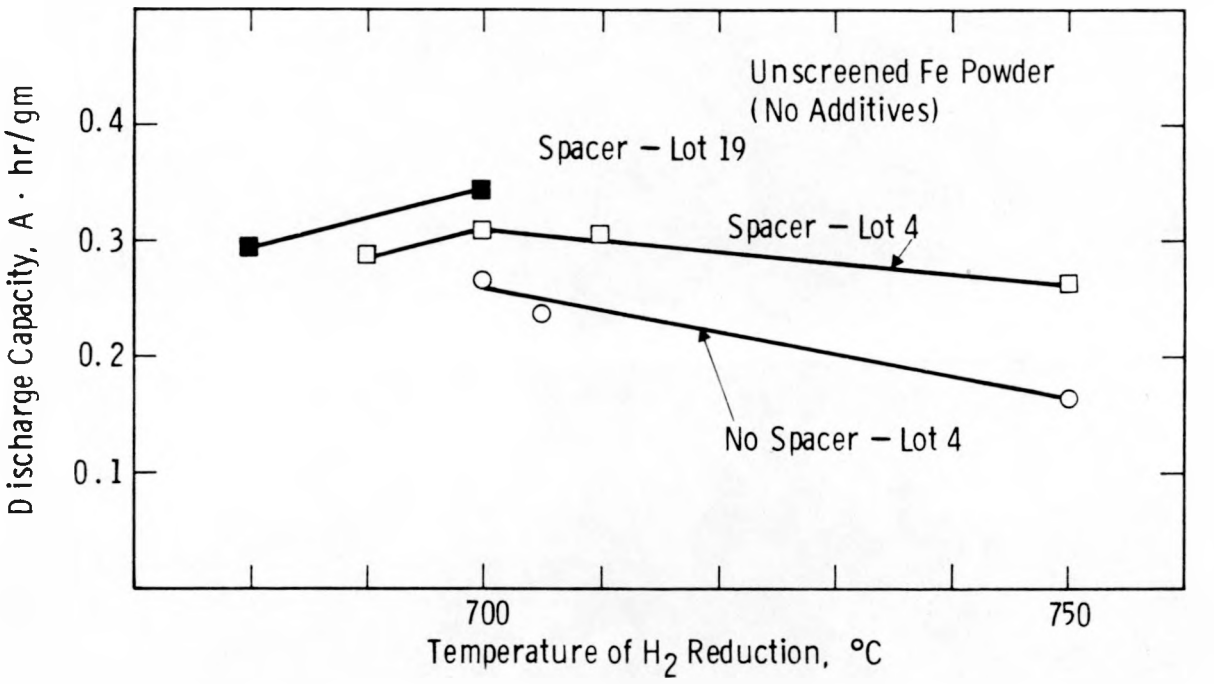

Figure 4-10: Influence of Fe_2O_3 Reduction Temperature on Iron Electrode Discharge Capacity.

processing difficulty was often encountered in the form of bond rupture between current collector and electrode during the sintering operation. On the other hand, particle sizing to retain only the minus 400 mesh iron particles (18 μm) coupled with the $CdSO_4 \cdot 8\ H_2O$ treatment (ST process) resulted in a discharge capacity of about 0.35 A·hr/gm. It should be noted that essentially the same discharge capacity resulted from the application of this dual activation treatment to iron powder prepared from lot 0 Fe_2O_3. Apparently, capacity differences traceable exclusively to Fe_2O_3 powder lot (entries 1 and 2 of Figure 4-8) are no longer found once the iron powder is given the $CdSO_4 \cdot 8\ H_2O$ treatment (entry 7 of figure 4-8). The third dual treatment (700°C hydrogen reduction coupled with particle sizing - RS) produced an electrode discharge capacity of about 0.37 A·hr/gm. This entry, (no. 8), of Figure 4-8 also shows that a discharge capacity of 0.41 A·hr/gm was achieved when iron powder was prepared from 700°C reduced, lot 19 Fe_2O_3 followed by sizing.

With the combined employment of all these activation treatments (RST, entry 9 of Figure 4-8) discharge capacities in excess of 0.4 A·hr/gm were realized. On cycle number 31 a discharge capacity of 0.48 A·hr/gm was obtained. With the substitution of lot 19 Fe_2O_3 for lot 4 Fe_2O_3 the capacity was also near 0.4 A·hr/gm.

In a further experiment using the RST treatment, an electrode was half-cell tested using about 1 to 2 cubic centimeters of electrolyte per gram of iron (compared to about 20 cc/gm Fe for the standard half-cell). The result for this smaller volume cell is given in entry 10 of Figure 4-8. The benefit of a smaller electrolyte volume was once again demonstrated but to a lesser extent than previously noted for electrodes prepared from less active iron powders.[1]

Selection of Sintering Parameters and Spacer

In the work described in the previous sub-section it was necessary to hold constant several of the process steps in order to limit the number of process variables to a manageable number. Specifically, sintering was limited to 10 minutes at 800°C and the amount and particle size of urea pore former was fixed at 10 volume percent and 115 microns (nominal) respectively. Blocks of experiments were run, using iron powder prepared by the RST process, to determine if these parameter levels were optimum.

With the only variable being sintering temperature (10 minute sinter time; 10 volume percent urea of 115 μm size), the data of Figure 4-11 were obtained. Based on 7th and 20th cycle discharge capacity, superior performance was noted for temperatures of 800°C to 900°C and the choice of 800°C for previous experiments was justified. The choice of sintering time of 10 minutes (about 50 minutes total furnace time) was found to be fortuitous based on the results of Figure 4-12.

Using the 10 minute at 800°C sintering schedule, electrodes were prepared having 10 volume percent urea but with urea particle size as a variable. The results of Figure 4-13 make it apparent that a nominal particle size of 115 μm was a reasonable choice even though the use of nominally 200 μm urea particles would have provided some improvement. The remaining variable of volume percent urea (for 115 μm nominal particle size) was evaluated as to its effect on electrode discharge capacity (Figure 4-14). Additions of urea spacer beyond 10 volume percent had no significant influence on discharge capacity.

Optimum Process for Iron Electrode Fabrication

With completion of the work on iron powder activiation, the RST process was selected for preparing electrodes for further evaluation (Section 4.3.3). In review, this process is as follows:

(R) Reduce Fe_2O_3 at 700°C in flowing hydrogen. [The Fe_2O_3 bed depth is limited to about 1/2 inch while the time at temperature is 30 minutes].

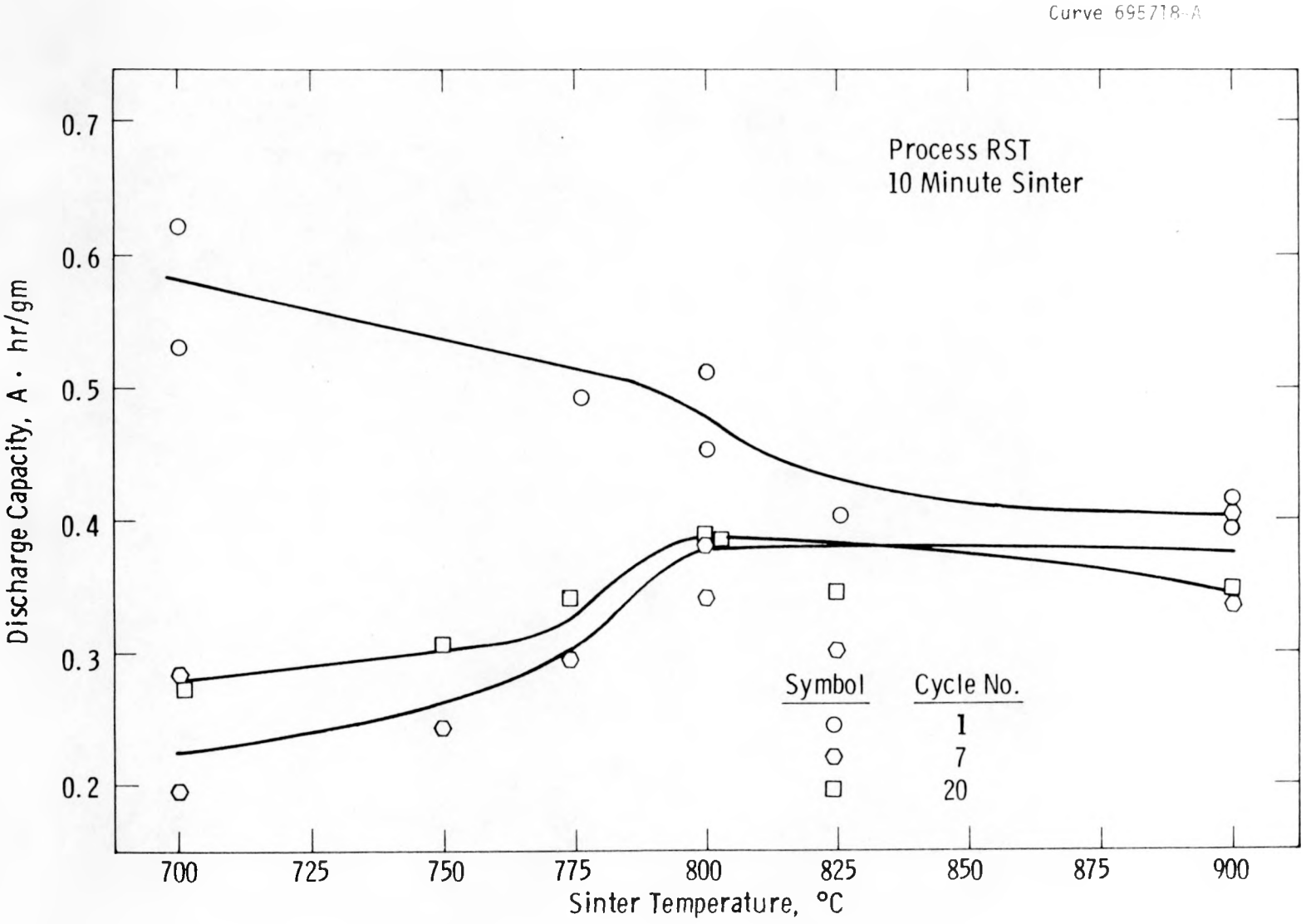

Figure 4-11: The Effect of Sintering Temperature on the Discharge Capacity of Iron Electrodes.

Curve 696669-A

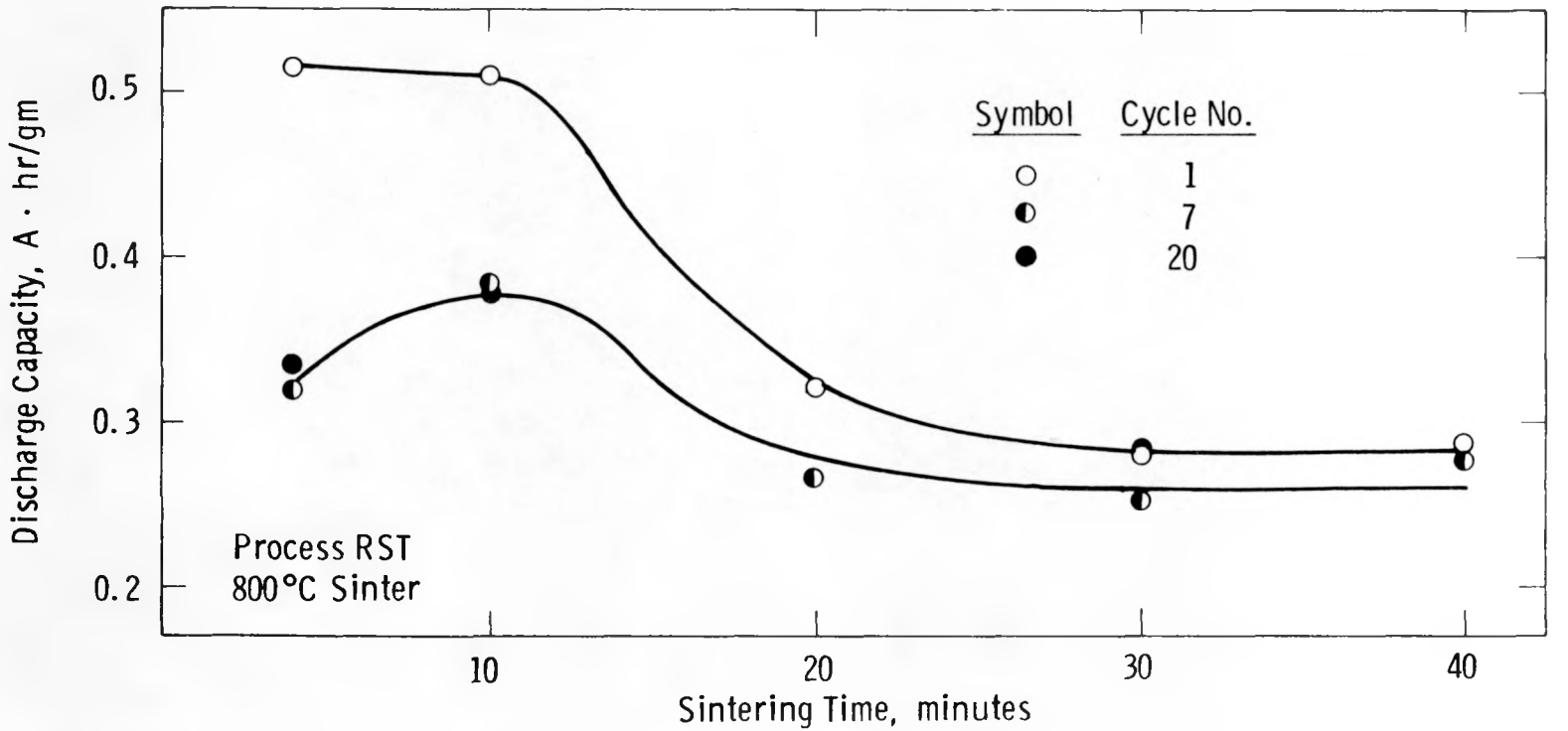

Figure 4-12: The Effect of Sintering Time on the Discharge Capacity of Iron Electrodes.

Curve 69-738-1

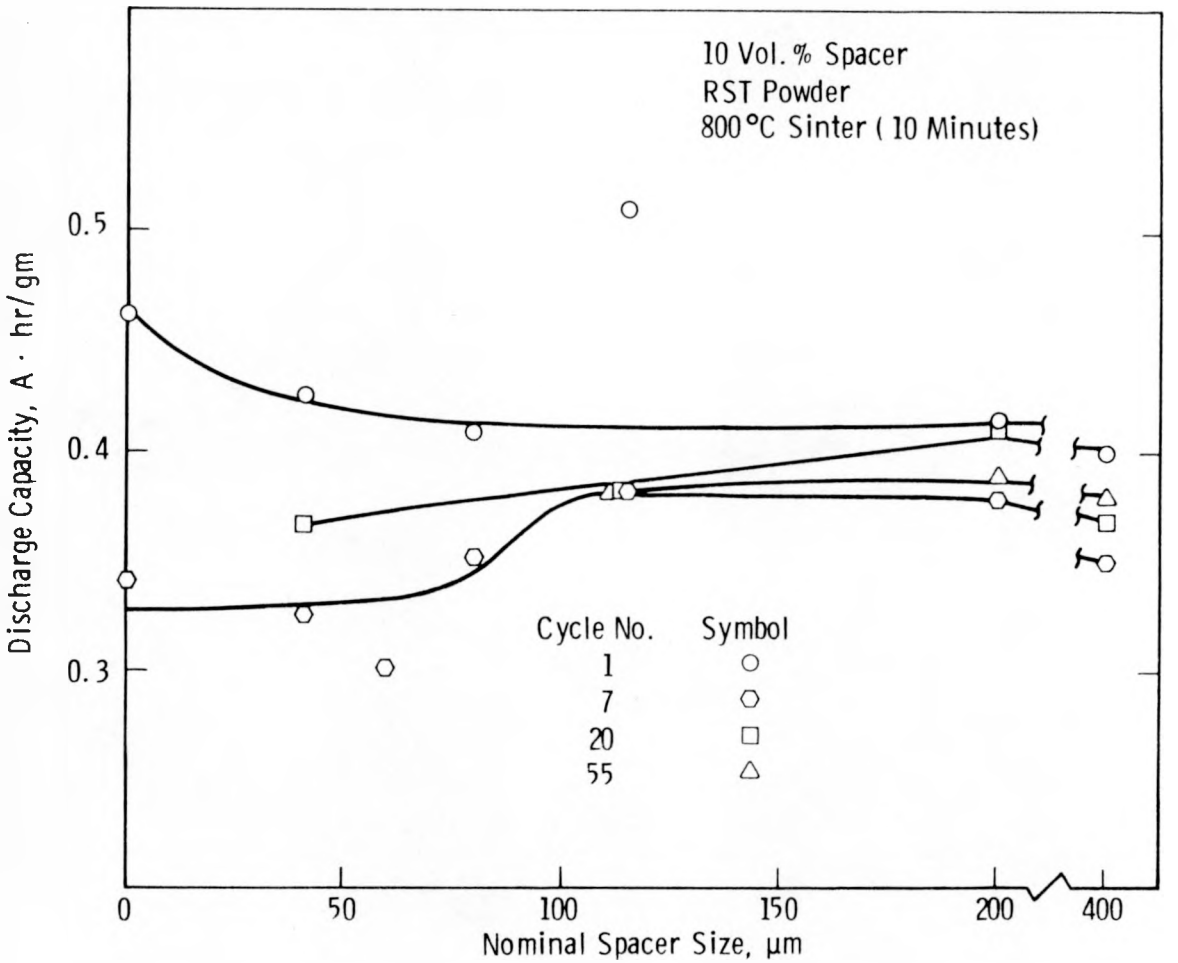

Figure 4-13: The Effect of Urea Particle Size on the Discharge Capacity of Iron Electrodes

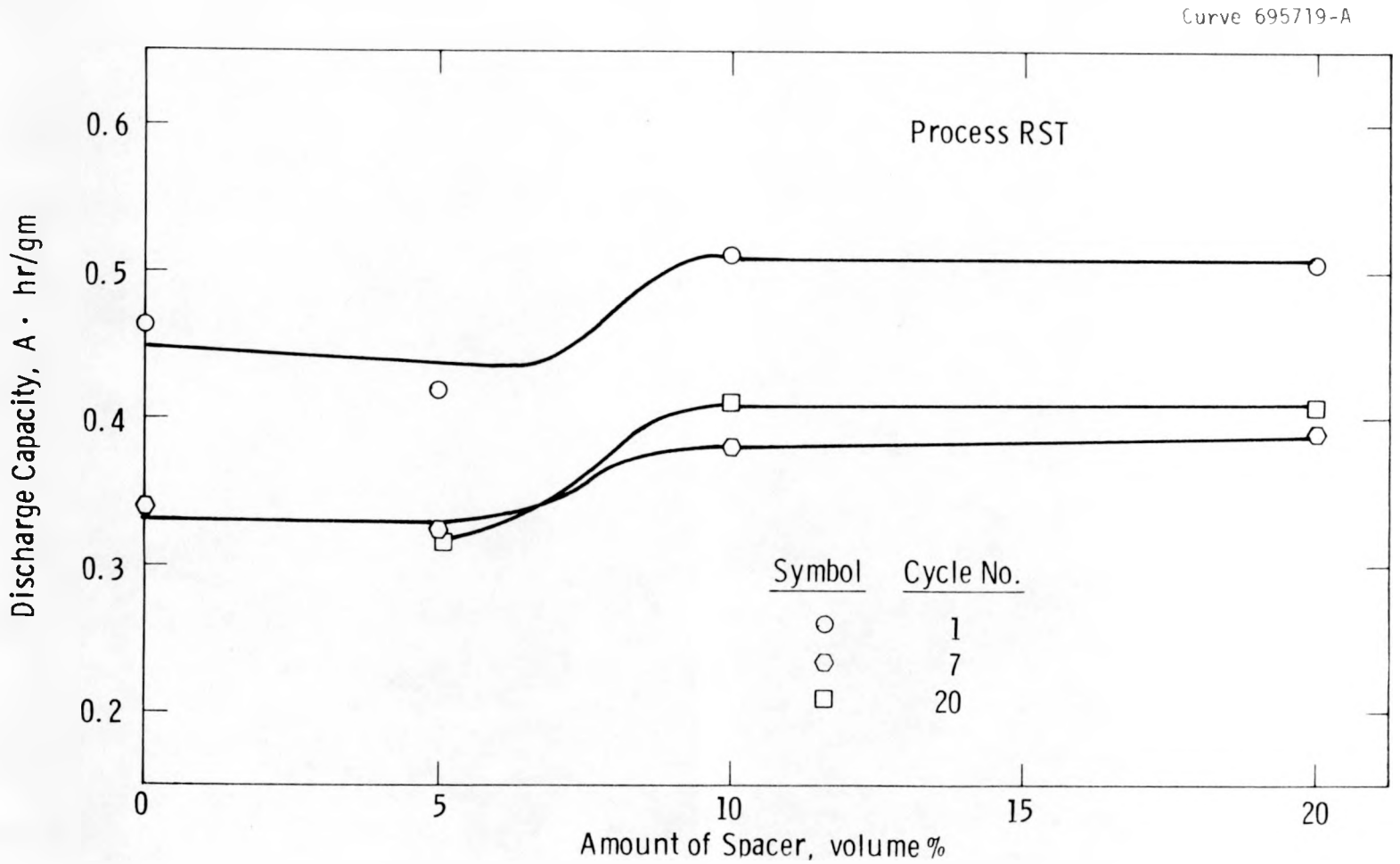

Figure 4-14: The Effect of Volume Percent Urea on the Discharge Capacity of Iron Electrodes

(S) Break up the loosely agglomerated iron powder by forcing it through a screen of between 60 and 100 mesh. The iron particles are then screened and separated according to size with only the smallest particles (less than 38 μm in size) reatained for further processing.

(T) A measured weight of less than 38 μm iron particles is mixed overnight in a rotating ceramic jar with about 10 parts by weight of deionized water and 2.4 weight percent (based on iron weight) of $CdSO_4 \cdot 8\ H_2O$. After mixing, most of the water is removed by decanting. Further drying to a caked mass is accomplished by heating in air at between 65°C and 80°C. The dried cake is crushed to powder by forcing it through a 60 mesh screen.

The activated iron powder is then dry blended with 10 volume percent (8.2 weight percent) urea of a nominal particle size of 115 μm (-100, +170 mesh).

A pre-weighed amount of the iron powder-urea mixture is pressed in a die cavity at about 3000 psi. Pressing is done in such a manner that the two major faces of the green electrode each contain a nickel mesh current collector. The current collector is 0.010 inches thick and contains 120 openings per square inch.

Sintering is carried out for 10 minutes at 800°C.

A sheet nickel current collector tab is spot welded to one of the current collectors.

Some future consideration will be given to two other processes. These include RS and R, but only with the use of a superior Fe_2O_3 powder lot such as lot 19. The former process eliminates the time-consuming water - $CdSO_4 \cdot H_2O$ treatment but, as noted previosly, it provided iron electrodes having superior discharge capacity (0.41 A·hr/gm) when lot 19 Fe_2O_3 powder was used. The R process produces fairly high capacity electrodes (0.35 A·hr/gm) when used with lot 19 powder and provides a further economy over the RST process since there are no oversized iron

particles to be discarded or to be reduced in size to smaller particles for later use.

Eventually, the choice will have to be made between using simpler iron powder processes which require a superior Fe_2O_3 powder or using a more involved process that does not require a superior Fe_3O_3 powder. The former choice will require either that we prepare our own Fe_2O_3 or find the means for specifying the properties required of superior Fe_2O_3 and convincing vendors that it would be worthwhile for them to produce such a powder. Choosing the more complicated RST process has obvious disadvantages, but would rid us of any dependence on technology that is either foreign to us (Fe_2O_3 preparation) or largely out of our control (selective Fe_2O_3 purchase).

Optimization of Fe Electrode's Density and Thickness

In a preceeding section of this report (4.1) a model describing the relation between an iron electrode's porosity and discharge capacity was presented. The model indicated that the optimum iron electrode density should be within the range of 20 to 25 percent of the theoretical density of iron (7.86 gm/cc). Even though densities within this range were used throughout the studies on iron powder activation (Section 4.3.2)) and a selection of sintering parameters and spacer (Section 4.3.2), it remained to experimentally verify the conclusion of the model.

Electrodes prepared by the RST process and having a sintered thickness of 0.093 inches (nominal), were fabricated to have a range of percent theoretical densities from 19.0 to 25.8. The twentieth cycle discharge capacities for these electrodes are given in the lower portion of Figure 4-15 where it can be seen that the maxima for theoretical discharge capacity and experimental discharge capacity both occur at about 22 percent of the theoretical density of iron (22% TD_{Fe}) or, alternatively, at 78 percent initial electrode porosity.

The data of Mitsumata et al.[4] on the capacity of iron-nickel cells (top portion of Figure 4-15) lends further support to the validity of the model since the maximum capacity values occur at very nearly equal values of initial porosity. The Mitsumata iron electrodes were about

Curve 695955-A

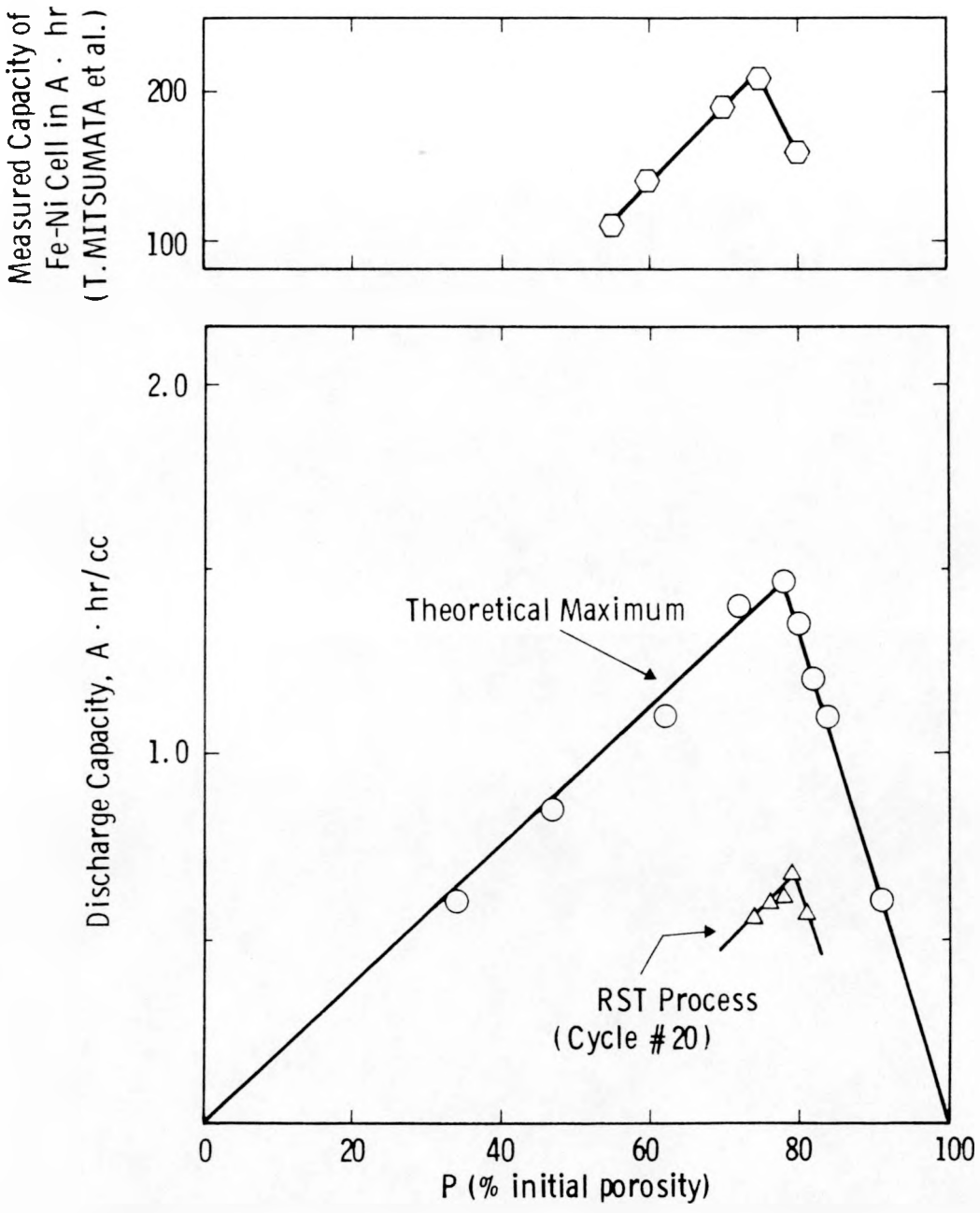

Figure 4-15: Optimum Density of Iron Electrodes Determined from Model and Experimental Data

0.040 inches thick. Therefore, as shown by the results to immediately follow, both sets of corroborating data were obtained with electrodes having thicknesses within the range over which the discharge capacity was essentially invariable with respect to thickness.

A projected design for the iron-air battery to be used for vehicle propulsion established the iron electrode thickness at about 0.100 inch. To assure ourselves that, indeed, this was an optimum thickness for electrodes 20 to 25% TD_{Fe}, a series of experiments was run to determine the relation between discharge capacity and electrode thickness. The results are presented in Figure 4-16. As electrode thickness was decreased from 0.150 inch to about 0.100 inch a large increase in 7th and 20th cycle discharge capacity was obtained. Further reductions in electrode thickness produced essentially no further change in discharge capacity for the 7th and 20th cycles. The design choice of 0.100 inch thickness was determined experimentally to be an excellent choice.

4.3.4 Fe Electrode Characterization

Electrode characteristics were determined for electrodes prepared from lot 4 Fe_2O_3 by the RST process (Section 4.3.2) and possessed of both optimum density and thickness (Section 4.3.3).

Percent electrode utilization was determined as a function of electrode potential and the data compared to that of Fukuda, et al.[5] for electrodes prepared from a number of starting materials and to that of an electrode prepared from our 1977 vintage sponge iron. These data are given in Figure 4-17. The activated Westinghouse sponge iron produced an electrode exhibiting 50% utilization (0.48 A·hr/gm) to a -0.75 volt cutout versus Hg/HgO. This marks an improvement over the best performance found by Fukuda, et al. for their FeOOH starting

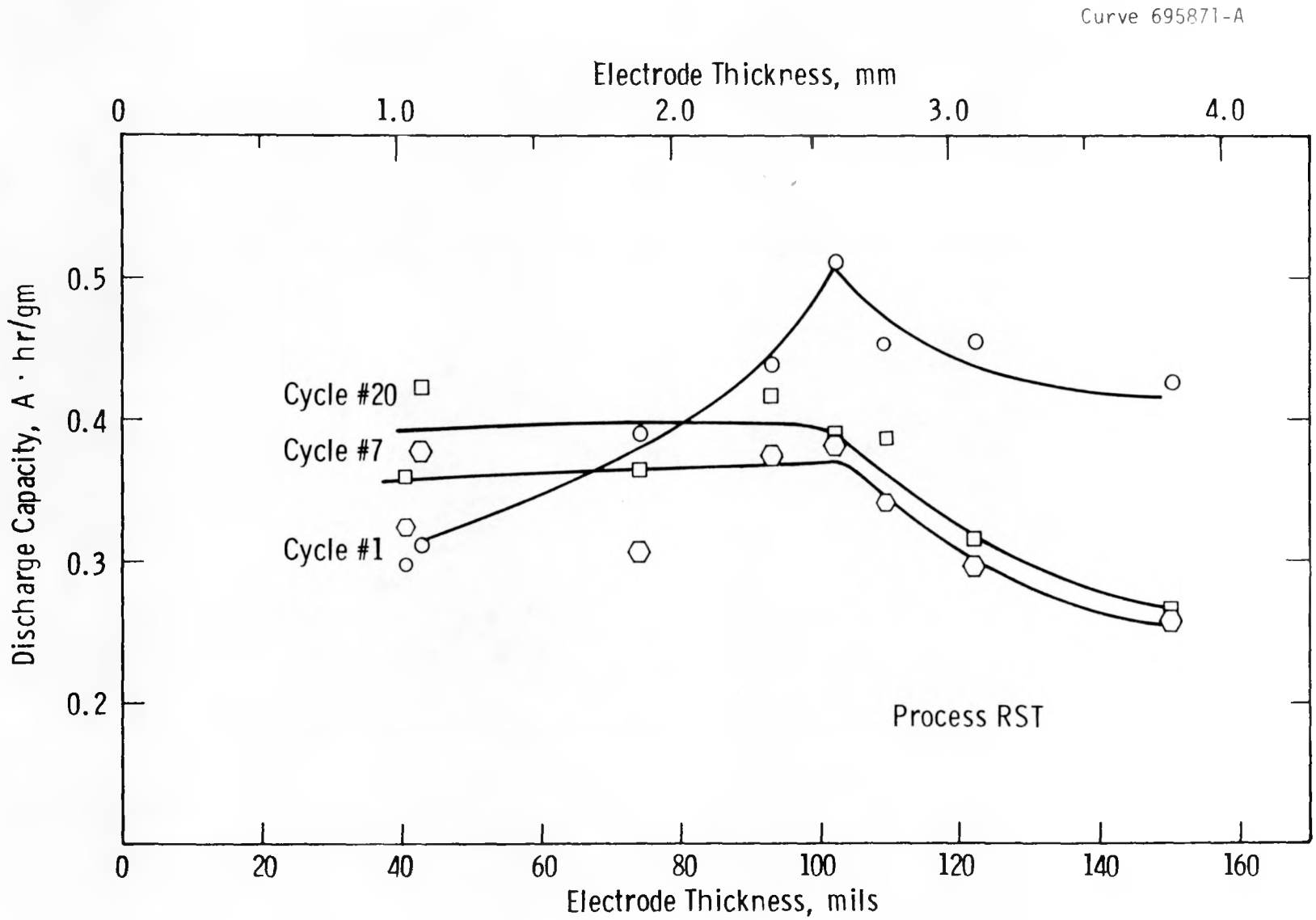

Figure 4-16: The Effect of Iron Electrode Thickness on its Discharge Capacity

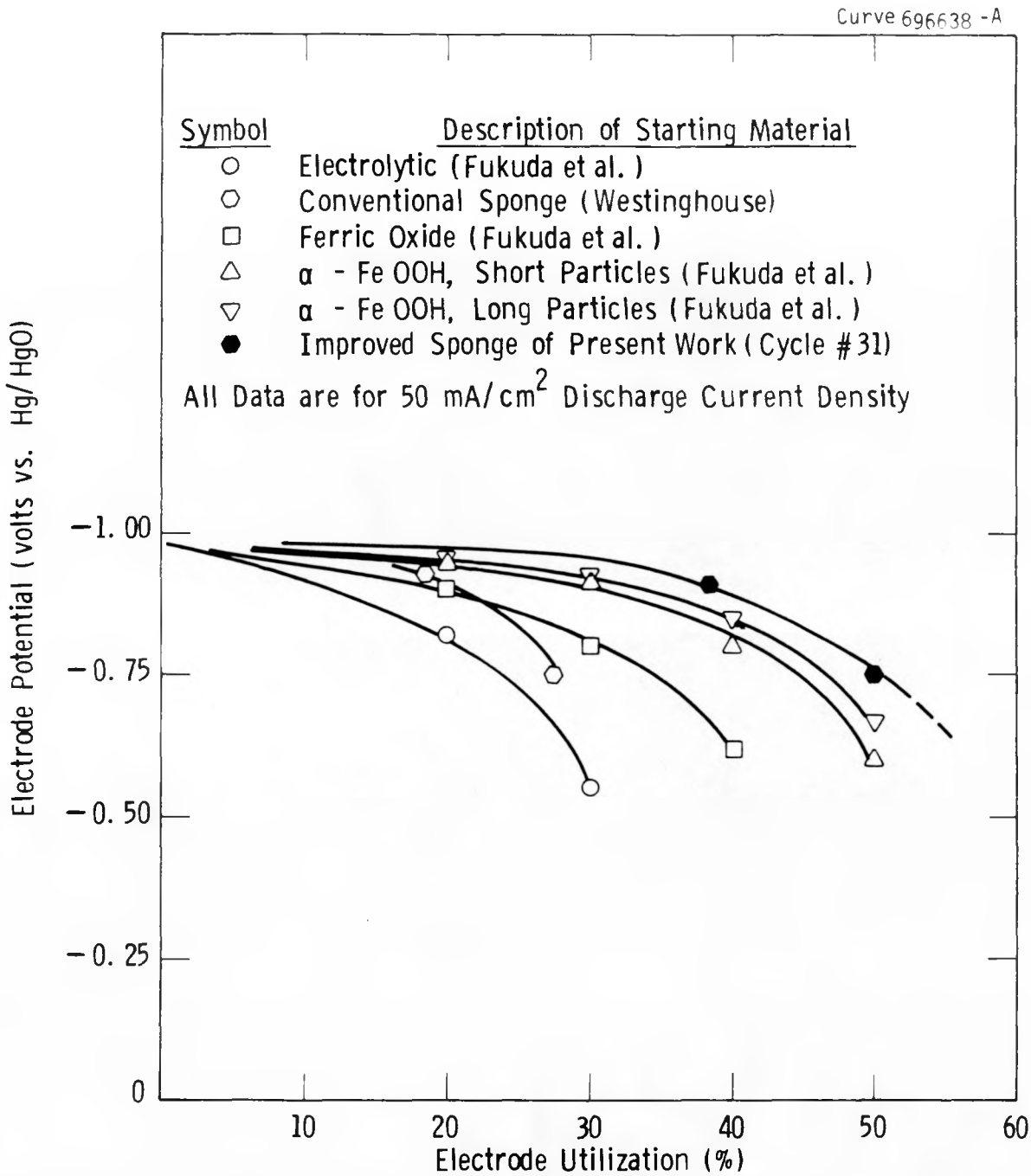

Figure 4-17: Utilization of Various Iron Electrodes

materials and a very decided improvement over the performance achieved with other starting materials, including our own 1977 sponge iron.

The discharge polarization characteristics for an RST electrode are shown in Figure 4-18. At 50 mA/cm^2 the voltage at the iron electrode is slightly better than the goal of -0.900 volts for this current density.

The effect of current density on discharge capacity is given by the data of Figure 4-19. Data for an electrode prepared by the ST process (i.e., identical to RST but with a 750°C hydrogen reduction instead of a 700°C hydrogen reduction) are also included because of the relative independence between variables which was found.

Figure 4-20 shows the discharge curve for an RST electrode. The discharge capacity to a cutoff of -0.750 volts (versus Hg/HgO) was 0.48 A·hr/gm for this particular half-cell cycle (number 31).

Electrode behavior characteristics for various half-cell conditions were evaluated. Several half-cell test conditions were evaluated as to their effect on the discharge capacity of RST iron electrodes. [The remaining test parameters were those given in the Procedure, Section 4.2].

In one test, (A), the half-cell temperature was limited to an average of about 35°C for the first three cycles, following which the usual test temperature of 44°C was employed. A duplicate, (B), RST electrode (0.093 inch thick) was maintained at 44°C throughout half-cell testing. Discharge capacity data for the two electrodes appear in Table IV-1. Not only did the low temperature used for the first three cycles reduce the performance of electrode (A) during that period but, in addition, subsequent performance was drastically reduced even though the temperature was restored to 44°C.

Curve 695733-A

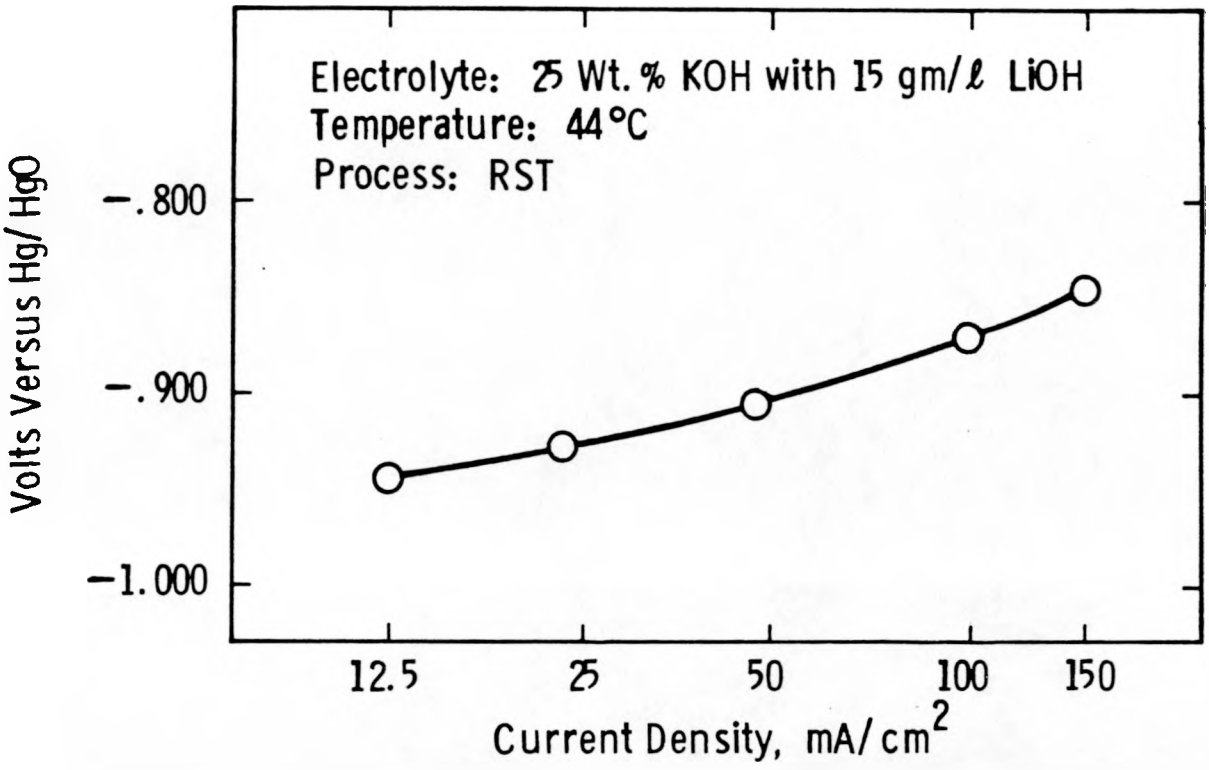

Figure 4-18: Discharge Polarization Characteristics of an Iron Electrode Prepared from RST Powder.

Curve 695736-A

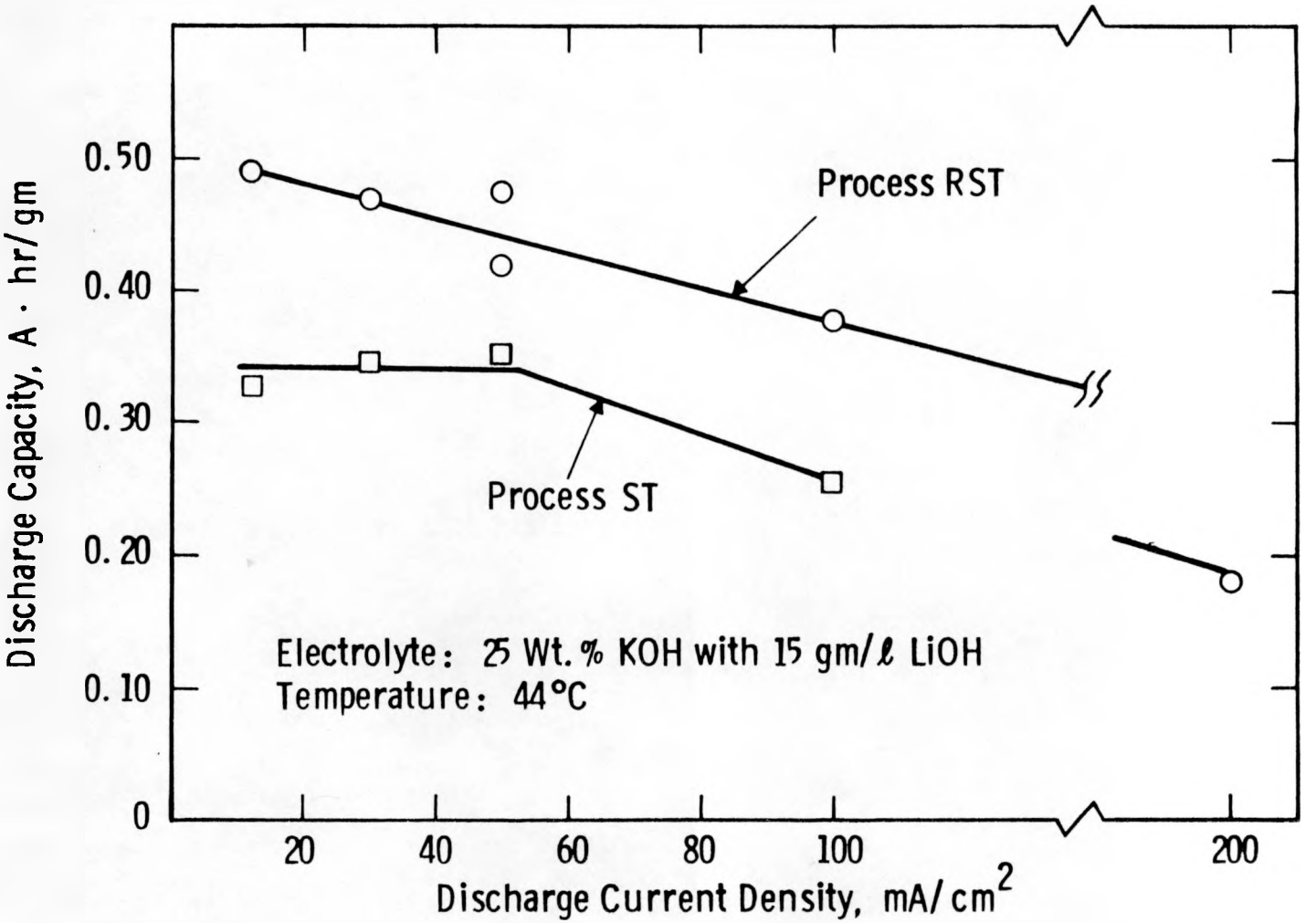

Figure 4-19: Discharge Capacities of RST and ST Electrodes at Various Current Densities

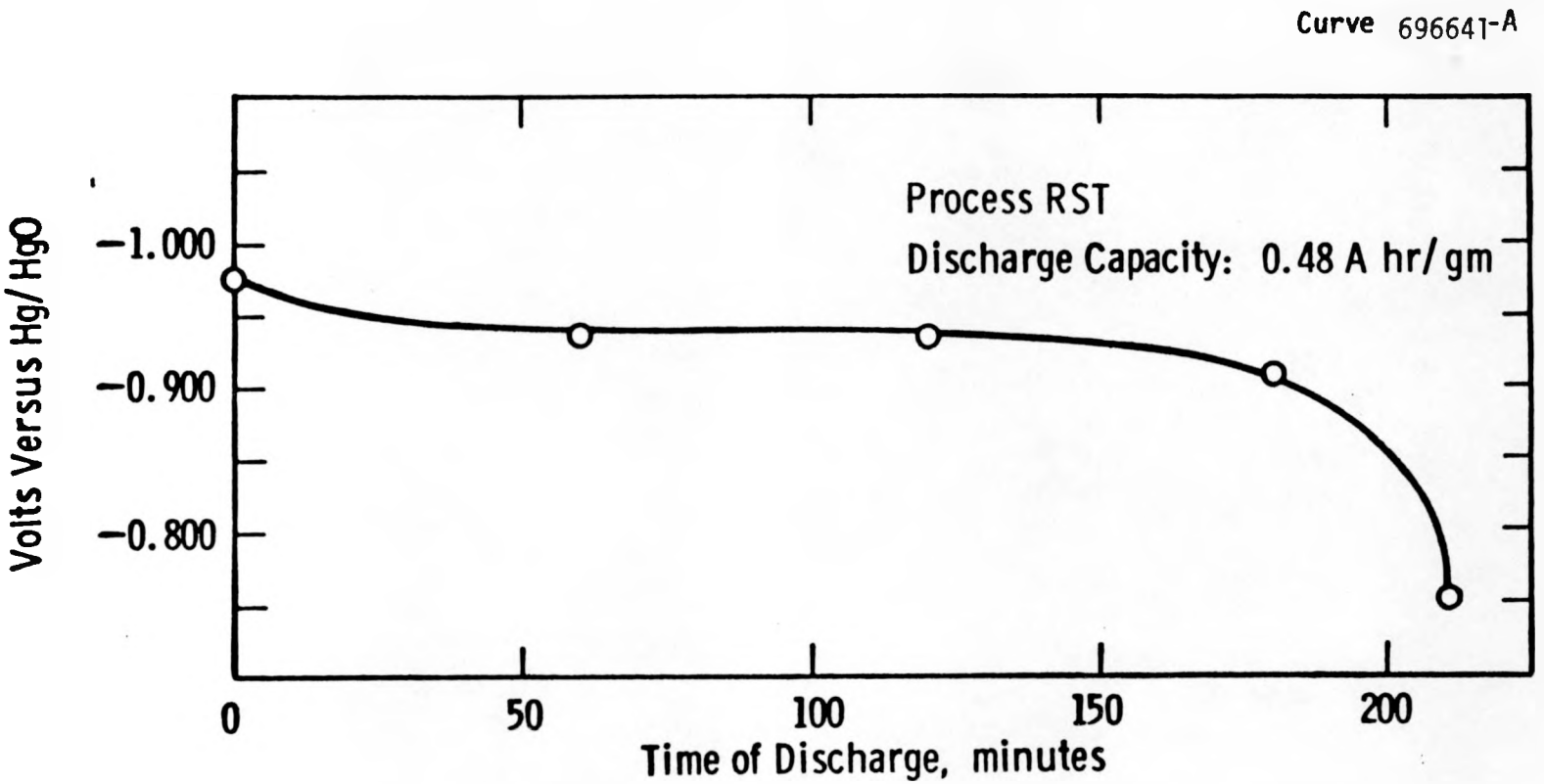

Figure 4-20: Discharge Curve for an Iron Electrode Prepared from RST Powder

TABLE IV-1 - INFLUENCE OF LOW TEMPERATURE EARLY CYCLES ON THE DISCHARGE CAPACITY OF IRON ELECTRODES

	Discharge Capacity (A•hr/gm)	
Cycle No.	Electrode A	Electrode B
1	0.378 (35°C)	0.439 (44°C)
2	0.201 (35°C)	0.318 (44°C)
3	0.219 (35°C)	0.316 (44°C)
7	0.297 (44°C)	0.374 (44°C)
20	0.334 (44°C)	0.418 (44°C)

The discharge capacity of an iron electrode is significantly affected by the concentration of KOH in the KOH-15 gm/l LiOH electrolyte (Figure 4-21). If air electrodes can be made to operate satisfactorily in more concentrated electrolyte, this extra iron capacity could be realized in iron-air cells. However, in the present contract period, the information from Figure 4-21 was used for another purpose. An RST electrode was half-cell tested for seven cycles in 45 weight percent KOH (15 gm/l LiOH). Following this initial test period the electrolyte was replaced with 25 weight percent KOH (15 gm/l LiOH) and cycling continued. The intent was to provide the electrode with a "memory" of high discharge capacity that would carry over once the more dilute electrolyte was used. The data of Table IV-2 suggest that the electrode possessed no such attribute since, once the more dilute electrolyte was substituted, discharge capacity fell to the value normally associated with this KOH concentration.

4.3.5 Continuing Efforts Toward Electrode Improvement

By the adopted criterion of 20th-cycle discharge capacity, electrodes prepared by the RST processing sequence performed very well. [Discharge capacities were generally in the range from 0.37 to 0.44 A•hr/gm.] With the goals of further improving the discharge capacity and the economics of powder processing, several studies were made.

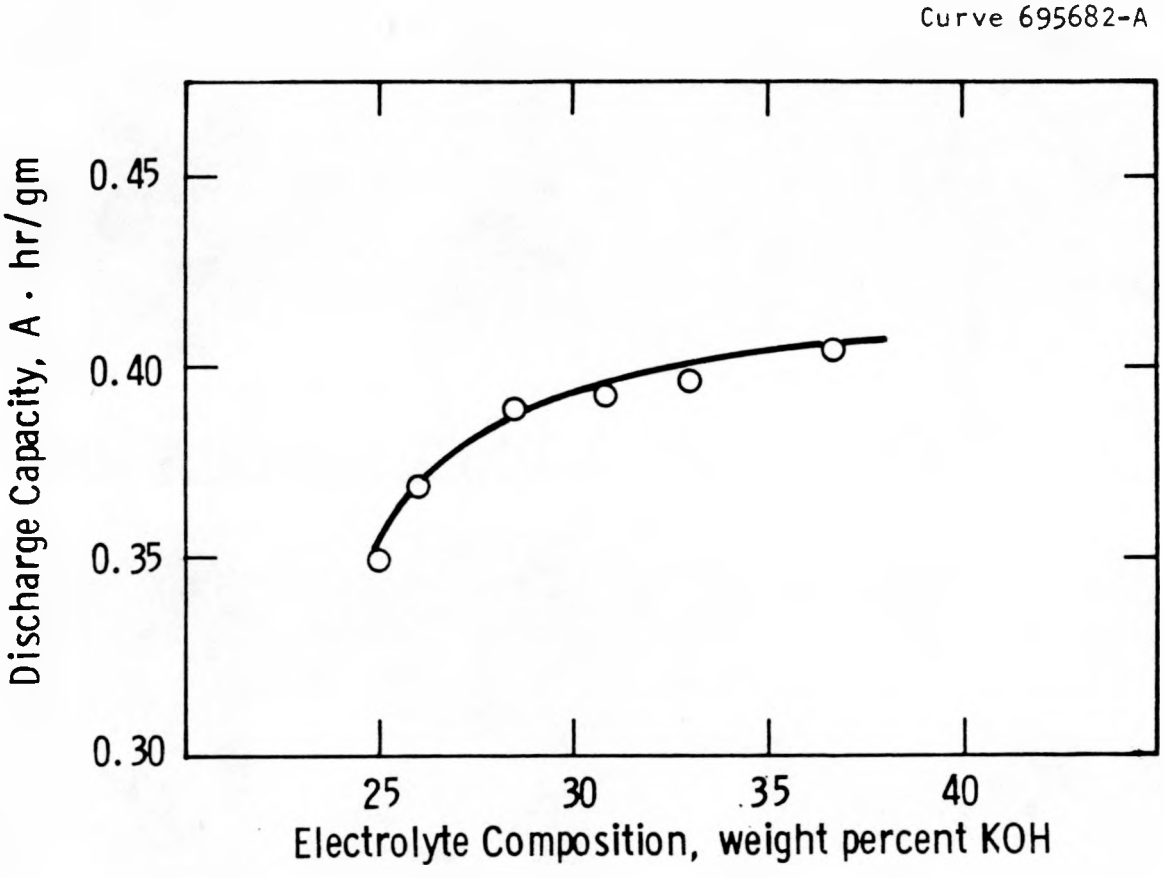

Figure 4-21: Discharge Capacity of an Iron Electrode in Various Electrolytes

TABLE IV-2 - IRON ELECTRODE DISCHARGE CAPACITY FOLLOWING CYCLIC STARTUP IN HIGHLY CONCENTRATED ELECTROLYTE

Cycle No.	KOH Concentration (w/o)	Discharge Capacity (A·hr/gm)
1	45	0.499
3	45	0.396
5	45	0.422
7	45	0.435
9	25	0.316
11	25	0.302

Further Studies on Sintering Parameters

Previously (Section 4.3.2) it was determined that maximum discharge capacity for RST electrodes was obtained at 800°C for 10 minutes at temperature. Other combinations of temperature and time of sintering were subsequently studied to determine if the capacity could be further improved. The data obtained appear in Figure 4-22.

Several results are apparent. For an 800°C sintering temperature- the optimum time at temperature is near 10 minutes. For 700°C sintered electrodes, 20th cycle discharge capacity (0.438 A·hr/gm) closely approached first cycle discharge capacity (0.46 A·hr/gm) and went through a maximum for a 60 minute sinter time. At greater times both first and 20th cycle discharge capacity decreased.

For 650°C sintered electrodes the point of maximum discharge capacity was not reached at sintering times up to 240 minutes. Although, from extrapolation to longer times, it appeared that discharge capacities equal to or in excess of 0.40 A·hr/gm could be achieved at this temperature, there was no economic incentive to experimentally confirm the observation.

Since the discharge capacity associated with a 60 minute sinter at 700°C is near the top of the range for RST electrodes sintered for 10 minutes at 800°C, further, duplicate testing of electrodes prepared by the former sintering schedule appear justified.

Curve 696662-A

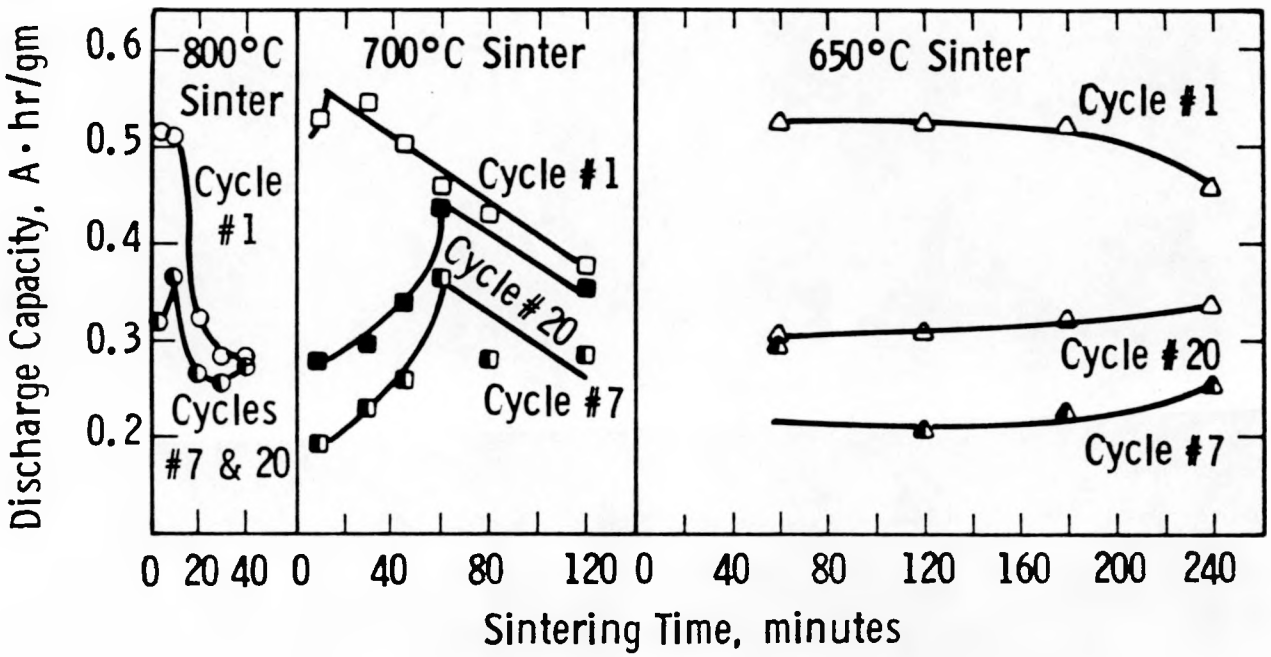

Figure 4-22: Discharge Capacity for Iron Electrodes Prepared with Various Sintering Times and Temperatures

Current Collector Improvement

On a total electrode weight basis (iron plus current collector) the discharge capacity of an RST electrode is about 0.3 A•hr/gm as compared to about 0.4 A•hr/gm on an active material only basis. The former property is of greater interest for battery design. Typically, the perforated nickel current collector comprises as much as 20 to 25 percent of the total weight of our iron electrode. Further reduction in discharge capacity (on a total weight basis) results from the shielding of portions of the electrode outer surface from the electrolyte by the current collectors. Efforts were made to increase this discharge capacity of RST electrodes by optimizing the current collector with respect to weight, type of material, form of material and location within the electrode. The results of our initial efforts are given in Table IV-3.

Electrode #1 contained 0.010 inch thick perforated nickel current collector on each of the two major faces. To date, this has been the usual configuration. Although the electrode's discharge capacity on an active weight basis is high, such cannot be said for its capacity on a total weight basis.

The first attempt at improvement (electrode #26) involved merely decreasing the weight of the external (major face) current collector. During the preliminaries to pressing of the electrode, one current collector was sheared into two pieces prior to its being placed in the die cavity. Following sintering, the larger of these two pieces of current collector, along with the one piece current collector on the opposite face, was peeled from the electrode. This operation left one face of the electrode partially covered with current collector and the other face completely free of current collector. [To provide the electrode with only this limited amount of external current collector prior to sintering would have produced a sintered electrode having non-uniform density and undesirable geometry (both the result of non-uniform shrinkage).] The Table IV-3 test results for electrode #26 show that elimination of the greater part of the external current collector is insufficient, in itself, to afford improvement in discharge capacity

TABLE IV-3 - IRON ELECTRODE CURRENT COLLECTOR DESIGN INNOVATIONS

Electrode Number	External (Face) Current Collector	Internal Current Collector	Weight in Grams of Internal Current Collector	20th Cycle Discharge Capacity (Ah/g of Active Weight	20th Cycle Discharge Capacity (Ah/g of Total Weight
1	Both Faces*	None	0	0.383	0.293
26	One Face, Partial**	None	0	0.340	0.329
37	One Face, Partial**	Ni Mesh***	0.3	0.342	0.309
39	One Face, Partial**	Ni Fiber	0.1	0.386	0.364
38	One Face, Partial**	Ni Fiber	0.2	0.402	0.372
42	One Face, Partial**	Ni Fiber	0.2	0.382	0.352
43	One Face, Partial**	Ni Fiber	0.4	0.400	0.352
44	One Face, Partial**	Steel Fiber	0.2	0.362	0.334

*Standard to date; the current collector is 10 mil thick nickel with 120 openings/in.^{2} and weighs 1.2 grams per 4.1 grams of iron.

**The current collector is 10 mil thick nickel with 120 openings/in.^{2} and weighs 0.15 grams per 4.1 grams of iron.

***The current collector is 5 mil thick nickel with 625 openings/in.^{2} and weighs 0.3 grams per 4.1 grams of iron.

(total weight basis) and, in addition, results in somewhat lowered discharge capacity (active weight basis). In succeeding experiments the partial external current collector was retained but in conjunction with another current collector placed in the interior (mid-thickness) of the electrode.

The first internal current collector tried was 0.005 inches thick, perforated nickel sheet having much finer openings than possessed by the partial, external current collector. Discharge capacity (total weight basis) was not significantly improved for this electrode (#37). For subsequent tests internal current collectors were sought which had greater surface area. Thus, nickel fiber, in the form of a loosely compacted pad, was incorporated within the interior of electrodes along the plane of mid-thickness. In each case (electrodes #39, #38, #42 and #43) the total weight basis discharge capacity was increased significantly (by as much as 27 percent) over that of the electrode having the "standard" current collector design (#1). No correlation was noted between the amount of nickel fiber current collector and the improvement in discharge capacity. Active weight discharge capacity was not sacrificed by the new collector configuration.

In an attempt to lower the cost of the internal current collector, steel fiber was substituted for nickel fiber (electrode #44). Total weight discharge capacity was once again significantly better than for the "standard" current collector design, but the improvement fell short of that achieved with nickel fiber.

Oxidation Reduction Studies of Sintered Electrodes

The success of the oxidation-reduction treatment applied to iron powder (process step T, Section 4.3.2). prompted a study of a similar treatment for sintered electrodes. An RS type electrode prepared from lot 19 Fe_2O_3 was chosen for testing. Heating in deionized water failed to produce any measureable degree of oxidation. Not until the temperature was raised to 200°C and the electrode was allowed to be contacted with air

was any noticeable oxidation achieved. Following reduction in hydrogen at 650°C, the electrode was half-cell tested. An identical, but untreated electrode (entry 8 of Figure 4-8) had a discharge capacity of 0.41 A·hr/gm. However, the discharge capacity of the oxidized-reduced electrode for its 20th cycle was only 0.26 A·hr/gm. No further oxidation-reduction treatment of sintering electrodes was attempted.

Fe_2O_3 Incorporation into Green Fe Electrodes

The much finer ultimate particle size of Fe_2O_3 compared to that of its sponge iron reduction product fostered the idea that, perhaps, replacement of a portion of the sponge iron in a green electrode with Fe_2O_3 might result in a more active sintered electrode. RST electrodes were prepared in which 25 percent of the iron in the sintered electrode was derived from Fe_2O_3 added to the urea-iron powder mix. Electrodes pressed at 3200 psi and sintered at either 700°C or 800°C for 10 minutes exhibited a large, single crack at about mid-width of the electrode. Increasing the green thickness and green density by simultaneously employing greater powder charge weight and greater pressing pressure produced a crack-free electrode following sintering for 10 minutes at 700°C. Its 20th cycle discharge capacity of 0.25 A·hr/gm compared unfavorably with RST electrodes prepared without Fe_2O_3.

Recovery of Oversized Iron Particles

For each powder preparation process involving a sizing operation there remains, following processing, a quantity of oversize iron particles. To see if they could be recovered for future use, previously sized, S process iron particles of greater than 60 mesh (250 micron) were dry ball milled overnight. Approximately 30% of the milled product was less than 400 mesh (19 micron). This fraction was given the oxidation (T) treatment and pressed into electrodes. Unfortunately, their green strength was insufficient to permit handling. The study will likely be continued at a future date since its success could eventually provide a significant contribution to the overall program.

4.4 DISCUSSION OF RESULTS

4.4.1 Iron Powder Activation

Three means of iron powder activation were employed in the contract period (June 77-May 78), i.e., particle sizing, reduced temperature of Fe_2O_3 reduction and an oxidation-reduction treatment. The improvement to discharge capacity resulting from the use of only the smallest iron particles (less than 400 mesh) undoubtedly is related in part to the increased total surface area provided to the electrode. [Smaller particle size is also known to favor increased rate of inter-particle neck growth which, in turn, would provide lower resistance to the electrode.]

No detailed explanation can be given at this time for the mechanism by which reduced temperature Fe_2O_3 reduction improved discharge capacity since no measurements were made of powders on electrodes by B.E.T., mercury porosimeter or SEM techniques. It is known, however, from the work of Turkdogan, et al.,[6] that a decrease in the temperature of hydrogen reduction of Fe_2O_3 from 800°C to 700°C can increase the surface area of the iron by a factor of almost two.

It was determined by X-ray diffraction that the oxidation portion of the oxidation-reduction treatment produced Fe_3O_4 and FeO at the iron surface. Perhaps reduction, during sintering, of the oxide film creates a defect structure in the iron which enhances its discharge capacity or which promotes interparticle neck formation during sintering to decrease the electrode's resistivity. Its more certain that the increased capacity is not the result of either cadmium or sulfur in the iron. Prior to the sintering (reduction) of electrodes prepared from the $CdSO_4 \cdot 8\ H_2O$ treated iron powder, their cadmium content was 4700 ppm. Following sintering, these electrodes contained only 0.26 ppm cadmium. Sulfur in the 800°C sintered electrodes was only 230 ppm (down from 2350 ppm in the treated powder). In low discharge capacity electrodes prepared from non-treated powder, the sulfur content was 130 ppm following sintering at 900°C. The slight difference in sulfur contents between these electrodes is attributed to the difference in sintering temperatures. Further support for the contention that discharge capacity improvement

resulting from the oxidation - reduction treatment is little related to either sulfur or cadmium incorporation is provided by the data of Figure 4-9. The difference in discharge capacities of electrodes prepared from $CdSO_4 \cdot 8\ H_2O$-treated and water-treated* powders is slight and is probably within the expected range of experimental error for the measurement of discharge capacity.

4.4.2 The Influence of Sintering Parameters on Discharge Capacity Through Changes in Surface Area and Interparticle Neck Growth

The Effect of Sintering Time

Reference to the left hand data of Figure 4-23 (redrawn from the 700°C data plots of Figure 4-22) suggests that two separate factors are controlling the dependence of discharge capacity on electrode sintering time. The portion of each curve which exhibits negative slope is indicative of the decreasing total surface area (the driving force for sintering) which accompanies longer sintering times. The portion of each curve for which the slope is positive suggests a dependence of capacity on the extent of interparticle neck formation. [The greater the thickness of necks formed between iron particles, the lower the resistance should be for the electrode.]

The latter hypothesis was tested as follows. Kuczynski[7] and, also, other investigators[8], have shown that the half-thickness of a neck formed during sintering (X) is related to time of sintering (t) by the relation

$$X \alpha t^{1/n} \qquad (1)$$

For alpha iron (the stable iron phase over our range of sintering temperatures) n has the value of 7. Therefore, if indeed one determinant of discharge capacity is the degree of neck growth, the positive sloped component of each left hand curve of Figure 4-23 should have a slope of

*Only iron powder and water were mixed and dried to form oxidized powder by this treatment.

Curve 696661-A

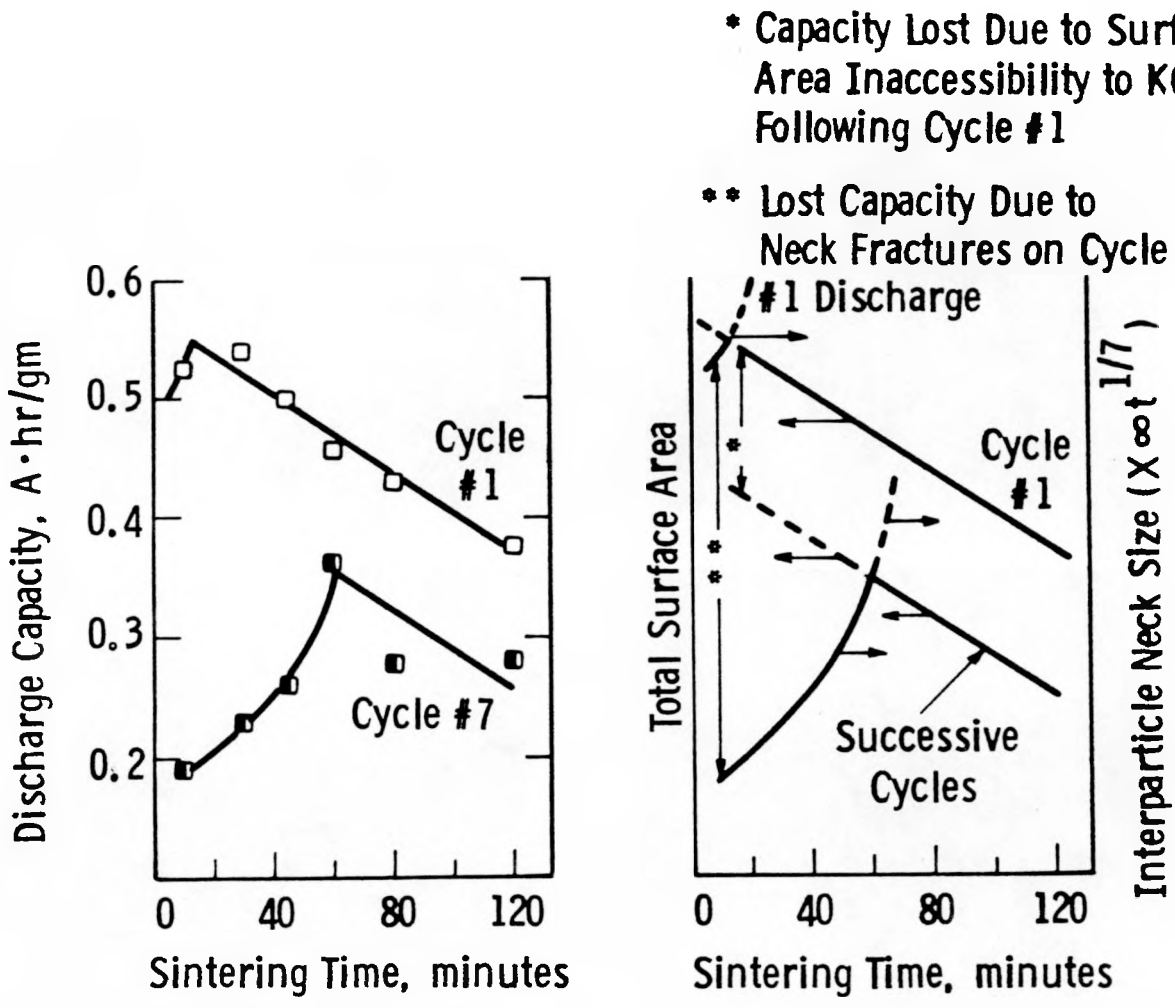

Figure 4-23 Proposed Relation Between Discharge Capacity and an Electrode's Total Surface Area and Interparticle Neck Size.

1/7 when replotted on a log-log basis. Figure 4-24 shows this plot. The lines drawn through each set of data have slopes of 1/7 and are seen to represent the data points fairly well, thus supporting the hypothesis.

The separate components of the Figure 4-23 discharge curves are redrawn in the right-hand portion of the same figure. For the first cycle, the number of inter-particle contacts and inter-particle necks would be expected to be very large. Therefore the limitation on discharge capacity due to internal electrode resistance would be small. As the cycle #1 curve shows, only for sintering times less than about 20 minutes is the first cycle capacity limited by electrode resistance (extent of inter-particle contacts and necks). However as first cycle discharge proceeds, many interparticle contacts (including necks) would be expected to be broken due to the product of discharge ($Fe(OH)_2$) having a greater molar volume than that possessed by iron. Only the stronger necks would remain following first cycle discharge and their thickness would determine, along with the active area remaining for the second cycle,* the discharge capacity for succeeding cycles. Thus, for the example of Figure 4-23, the discharge capacity of successive cycles is limited by the extent of retained inter-particle necks for electrode sintering times of up to about one hour. For greater sintering times the amount of remaining active area limits the discharge capacity. Note that, for sintering at 700°C, the loss in capacity from that of cycle #1 due to active area loss is not nearly as great as that from neck fracture in their respective regimes of capacity limitation.

At a sintering temperature of 650°C, as shown by the data of Figure 4-22 , discharge capacity beyond the first cycle was limited, for all sintering times to 4 hours, by the iron electrode resistance (extent of retained neck formation). At a sintering temperature of 800°C, a sintering time of 10 minutes is sufficient to change control of

*In a previous report[1] it was shown that only the area associated with pores of greater than about one micron was available (remained active) for longer than the first cycle.

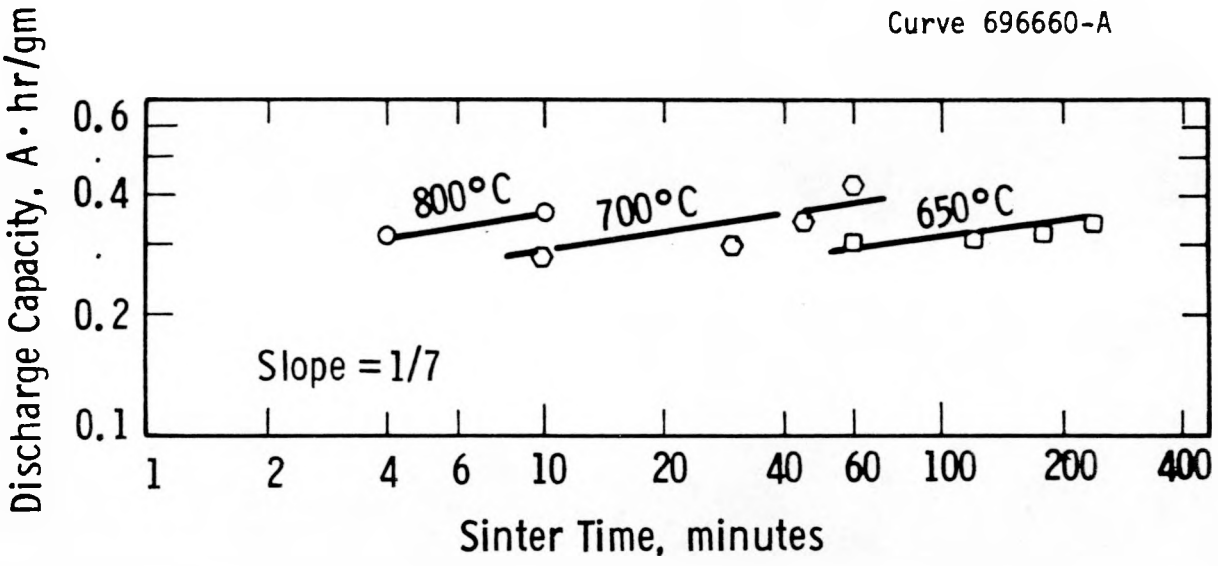

Figure 4-24: Discharge Capacity (Interpartical Neck Size) as a Function of Sintering Time

successive cycle discharge capacity from retained neck formation to retained active area. The loss in active area from the first cycle is relatively slight since much of the area associated with greatest curvature (smallest pores) would already have been dissipated by the sintering treatment.

It is also evident from Figure 4-22 that as the sintering temperature decreases, the increase in capacity between the 7th and 20th cycles is generally greater. During the intervening cycles the KOH concentration increases somewhat. Obviously, though, other factors must be involved, since KOH concentration change alone cannot explain the behavior. For every size pore, at the start of discharge, a critical number of OH^- ions must be contained within to permit full utilization of the iron comprising the walls of the pore. It is reasoned, therefore, that the largest pores can operate fully on KOH of either the starting concentration of 25 weight percent (represented by cycle #7) or the increased concentration of about 35 wt. percent (represented by cycle #20). However the smallest pores would be expected to operate to their fullest extent only with the more concentrated electrolyte. It is reasonable to suggest that decreased sintering (lower sintering temperature) has permitted retention of many of the smallest pores that would otherwise have been eliminated through the greater reduction in surface area which would have accompanied increased sintering at a higher temperature.

The Influence of Sintering Temperature

For RST powder, the effect of sintering temperature (constant 10 minute sintering time) on discharge capacity was shown by the data of Figure 4-11. In general, these plots have the same shape as those given by the model suggested for the effect of sintering time (Figure 4-22). First cycle discharge capacity decreases with more extensive sintering (greater reduction of total surface area) but only up to about 800°C. For later cycles, the discharge capacity for less severe sintering (temperatures up to about 800°C) is limited by the extent of interparticle bonds (necks) which determine the electrodes

electrical resistance. However, later-cycle capacity does not fall off for higher sintering temperatures (800°C and greater) as suggested by the model. The deviations from the model which occur for electrodes sintered above about 800°C can be explained by noting that as the sintering temperature begins to approach the $\alpha - \gamma$ transformation temperature the self-diffusion coefficient for iron drops very rapidly. In turn, as shown by several investigators[9,10], the sintering rate for iron powder remains fairly constant and even may decrease (depending upon particle size and powder type) over the 800°C to 900°C range.

For electrodes prepared from sized and treated iron prepared from 750°C reduced Fe_2O_3 (ST process) the dependence of discharge capacity on sintering temperature is much the same as for RST powder (700°C Fe_2O_3 reduction) as indicated by the results of Figure 4-25. At the higher sintering temperatures (825°C and greater) the discharge capacity of ST electrodes is practically independent of cycle number. This indicates that there are relatively few very small pores(<about one micron in diameter) in the as-sintered electrode. [From previous arguments, it will be recalled that it is these pores which are inaccessible to electrolyte following first cycle discharge and which are responsible, along with KOH concentration increase, for the often observed increase in capacity from the 7th to the 20th cycle.* Thus, in the absence of these small pores, discharge capacity is essentially independent of cycle number.] For the same sintering temperature range (and perhaps at lower temperatures as well), electrodes prepared from RST powder (700°C Fe_2O_3 reduction) show some dependence of discharge capacity on cycle number (Figure 4-11). Apparently, therefore, the benefit derived from lower temtemperature reduction of Fe_2O_3 is to provide the iron powder (and the electrode) with a greater proportion of smaller pores that is sufficient to permit their retention, in part, during the sintering operation.

---

*At completion of the 7th cycle water was added to restore KOH concentration to its original, first cycle value.

Curve 695737-A

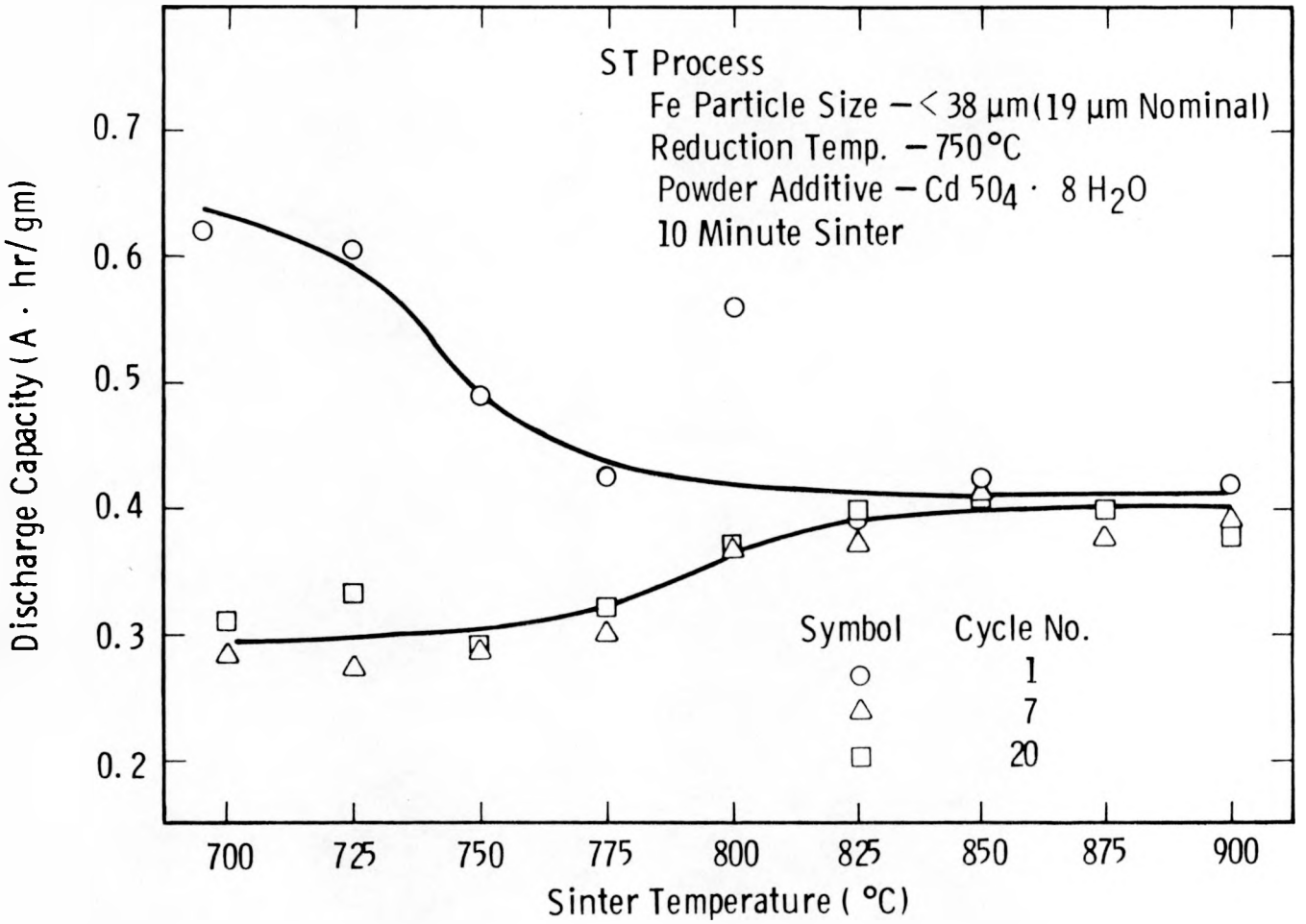

Figure 4-25: The Effect of Sintering Temperature on the Discharge Capacity of Iron Electrodes Prepared from ST Powder.

4.5 SUMMARY

Significant progress was made in this reporting period. The discharge capacity at a current density suitable for an iron-air battery for vehicle propulsion (50 mA/cm^2) was increased from about 0.27 A•hr/gm to 0.4 A•hr/gm and higher. This improvement resulted from several changes made to the iron powder processing, namely sizing to yield only less than 38 micron particles, reduced temperature of Fe_2O_3 reduction from 750°C to 700°C, incorporation of the oxidation-reduction treatment and the use of urea as a pore-forming agent. A study of the sintering operation to include the separate effects of time and temperature produced a sintering schedule (60 minutes at 700°C) which produced an electrode (prepared by the improved method of powder processing) having a discharge capacity of 0.44 A•hr/gm.

The goal of 0.4 A•hr/gm discharge capacity was also achieved by a simpler variant of the new powder processing procedure in which the oxidation-reduction treatment was eliminated. However, in this instance, a superior Fe_2O_3 starting material (lot number 19) had to be used.

The discharge capacity of electrodes prepared by the improved process was optimized with respect to electrode density and thickness. The greatest capacities (20th cycle) were associated with a density of 21% TD_{Fe} (0.41 A•hr/gm) and a thickness of 0.093 inches (0.42 A•hr/gm).

Although these discharge capacities are high (especially when compared to those being achieved a year or so ago), on a total weight of electrode basis some improvement was desirable. This improvement (from 0.29 A•hr/gm to as high as 0.37 A•hr/gm) was accomplished by preparing an electrode which, in its final form, contained much less current collector and had a portion of it in the interior of the electrode.

The target discharge voltage (at 50mA/cm^2) of -0.90 volts versus Hg/HgO was bettered (-0.91 V) with an electrode made by the improved powder processing procedure. Charge voltages of -1.1 volts versus Hg/HgO for the 2 hour change rate (100 mA/cm^2) have been achieved also.

Consideration of a simplified model of iron particle sintering lent some insight into the processes occurring during electrode discharge. It is important that sintering proceed to an extent sufficient to provide considerable neck growth but not to an extent which would dissipate too much of the iron powders total surface area. Satisfaction of the latter condition requires that the powder have extensive surface area. Preferably this area will be associated with pores of one micron diameter or greater, since it has been found in our work that the area associated with smaller pores is active for only the first discharge of an electrode.

The maximum possible discharge capacity of an electrode was determined as a function of its initial porosity using a model formulated by Selanger.[2] This capacity, approachable only under ideal cell-testing conditions and with electrodes having both high total surface area and low resistance, is shown in Figure 4-26. Also included are some experimental values both from our own work and that of others[11-13]. Both our improvement during the past year and our iron electrodes excellent performance compared to those of other investigators are demonstrated.

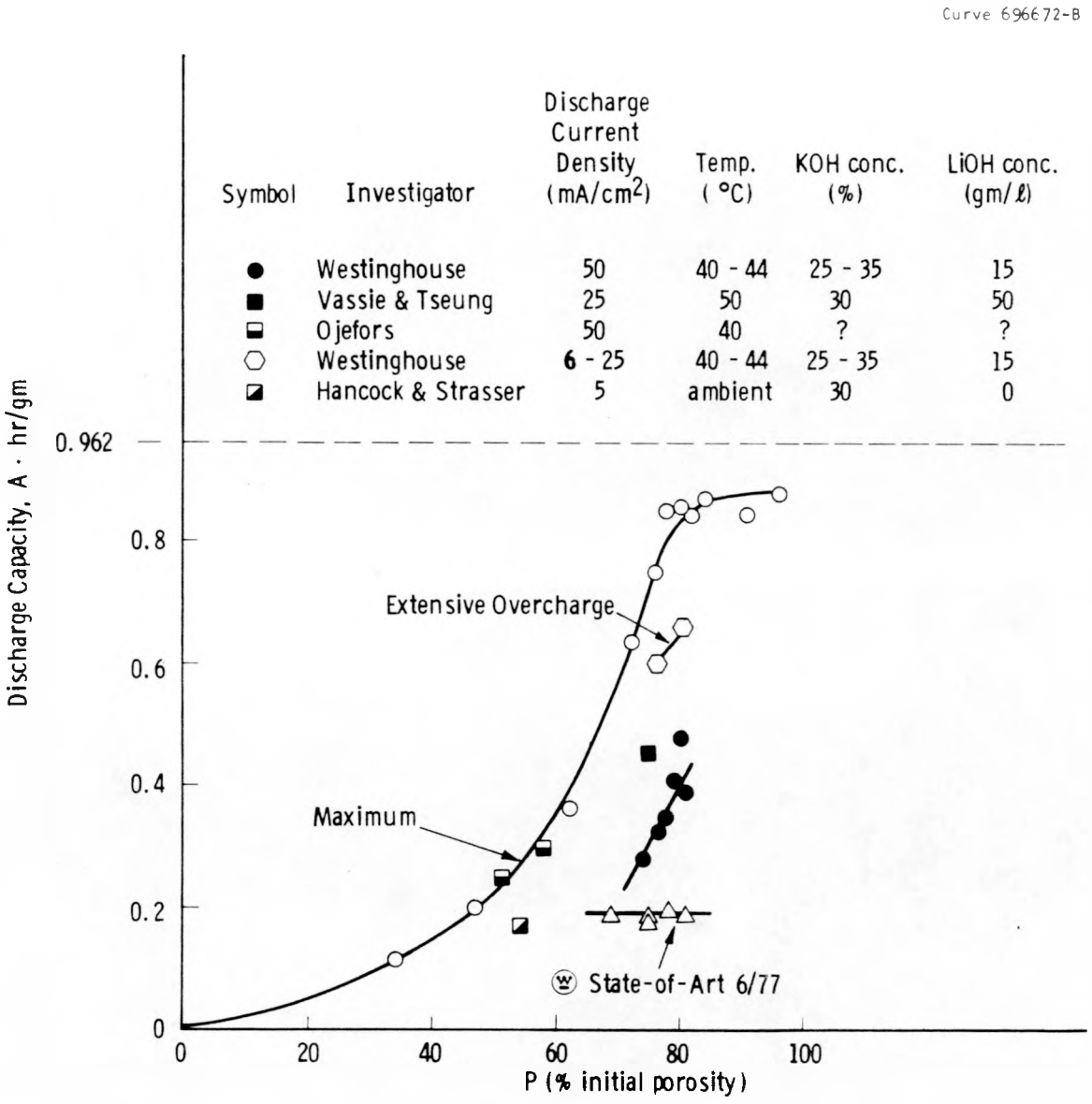

Figure 4-26: Comparison of Iron Electrode Maximum Discharge Capacity and the Experimental Discharge Capacity for Iron Electrodes Prepared by Several Investigators.

V. CELL STUDIES

5.1 Cell Testing Program

Iron-air cell studies have been mainly concerned with the demonstration of the electrical performance characteristics of the cell. All cells to be described were 100 cm^2 size cells. Early cell tests designed to simulate the expected use conditions of limited electrolyte and lightweight cell cases were short-lived due to mechanical problems. As a result of these failures, the cell configuration has been modified. The cell design presently in use is intended to demonstrate the electrical characteristics of the cell without regard for specific energy content, or specific power. The cell case is made of 1/8" ABS plastic with double, Delta Bond cement seals around the air electrode window. This configuration provides the mechanical integrity to prevent leaks but is overweight with respect to anticipated cell needs. Future design and engineering efforts to properly match the cell construction design and materials will produce appropriate lightweight cell cases.

Early iron-air cells which were tested in ambient air were found to pick up CO_2 from the air and dilute the electrolyte concentration by the formation of potassium carbonate. The result of this electrolyte depletion or contamination is a loss of capacity or charge acceptance in the iron electrode. This CO_2 pick-up by the electrolyte required periodic replacement of the electrolyte to maintain proper concentration conditions. Earlier life tests of air electrodes in half cells tested in ambient air did not display any adverse effects due to the CO_2 pick-up by the electrolyte. As a result of this problem, of testing in ambient air, we have chosen to run all iron-air cells in a CO_2-free atmosphere. Cell test chambers have been built which provide a CO_2-free environment. The air, which is fed into the chamber is first passed through a KOH solution-bubbler to remove the CO_2. The chamber is also equipped with electrical heaters and an automatic temperature controller to maintain 40°C. This temperature is approximately what is expected to be seen in a battery when it is used in an electric vehicle. The use of the heated, CO_2-free chambers simulate more realistically the use conditions which the iron-air cell will eventually see in a commuter electric vehicle.

5.2 Cell Testing

The testing of 100 cm^2 iron-air cells is carried out automatically, with the ability to cycle continuously, seven days a week. The cell cycler is programmed to charge the cell, or cells (up to twelve stations) at a preset constant current for some time, up to 16 hours. Once the preset time of charge has elapsed, the cells go immediately into discharge at a constant current. The discharge proceeds until the cell voltage drops to a predetermined cutoff voltage which represents 100% of the iron electrode capacity on the upper voltage plateau. The cell is then returned to the charge mode repeating the cell test. During the cell charge and discharge process, the cell voltage is monitored on a high impedance strip charge recorder. This provides a visual display of the voltage profile of the cell. At any time during either the charge or discharge mode, the cells may be polarized by mechanically changing the current and recording the resultant voltage charge of the cell. The cell cycler has a current range of 1 to 100 amps and can accommodate either single cells which are presently being tested or multi-cell modules which are expected to be tested in the future.

The data which are collected and recorded in the cell test program are the cell charge voltage and discharge voltage as well as the amp-hour input and output. This data then provides the voltage efficiency and the current efficiency of the test cycle. The cell discharge voltage and its reproducibility on repeated cycles gives an indication of the cells stability. The cell configuration and the CO_2-free test chamber have the added provision of using a Hg/HgO reference electrode to monitor the performance characteristics of the individual electrodes independently during any time of the cell test.

The cell tester, and the test program on the iron-air cells are intended to demonstrate the life characteristics of the iron-air couple under expected use conditions. These use conditions are expected to be an eight to ten hour charge with a four hour discharge. Our test program uses these charge-discharge times as the cyclic routine to evaluate the efficiency and stability of the iron-air cells.

5.3 Cell Test Results

Increased effort has been placed on the cell test program during the first half of this year's work. The standard cell size for evaluation is 100 cm^2 with each unit cell containing two air electrodes and one iron electrode. In the early phase of the test program, attempts were made to build cells which would simulate a high energy content iron-air cell. This design had lightweight, .010" thick cell cases and contained restricted, small amounts of electrolyte. After several of these cells failed due to excessive electrolyte leaks at cell joints, it was decided to alter the cell design to eliminate the mechanical problems and concentrate on the performance characteristics of the electrodes. In order to overcome the mechanical problems, we were forced to heavier cell case construction materials, along with a cell which contained more than the desired amount of electrolyte. After the successful demonstration of stable cell performance, a design and engineering program will be initiated to properly provide a cell case for the next scale-up to 400 cm^2 size cells. It is not within the scope of the present program to provide the necessary design and engineering effort required to do this task.

The objectives and goals for the Cell Development Program are given in Table 5-1. Clearly, the most important objectives at the present time are the demonstration of cyclic voltage efficiency and energy efficiency along with stable cycle life.

The objective to demonstrate the required power characteristics may be more related to cell design and may not be accomplished in the cell test configuration in use. It is expected that a properly engineered cell will have lower internal resistance and will demonstrate the expected power goal for the system.

Figure 5-1 shows the individual electrode polarization characteristics of the iron and air electrode against a Hg/HgO reference electrode in cell #36 after 15 cycles. It can be seen from this figure that the air electrode had a voltage of -.060 volts at 25 mA/cm^2, -.107 volts at 50 mA/cm^2 and -.230 volts at 150 mA/cm^2. These voltage performance levels for the air electrode are better than our established goals which were -.100 volts at 25 mA/cm^2; the expected cruise condition in an electric vehicle.

Table 5-1

CELL DEVELOPMENT PROGRAM

• Demonstrate Cell Power Characteristics	$\sim$70 mW/cm^2
• Demonstrate Electrode Performance in Cells	As in Half Cells
• Demonstrate Cyclic Voltage Efficiency	$\sim$50%
• Demonstrate Cyclic Energy Efficiency	$\sim$45%
• Demonstrate Cell Life	>100 Cycles

Curve 693229-A

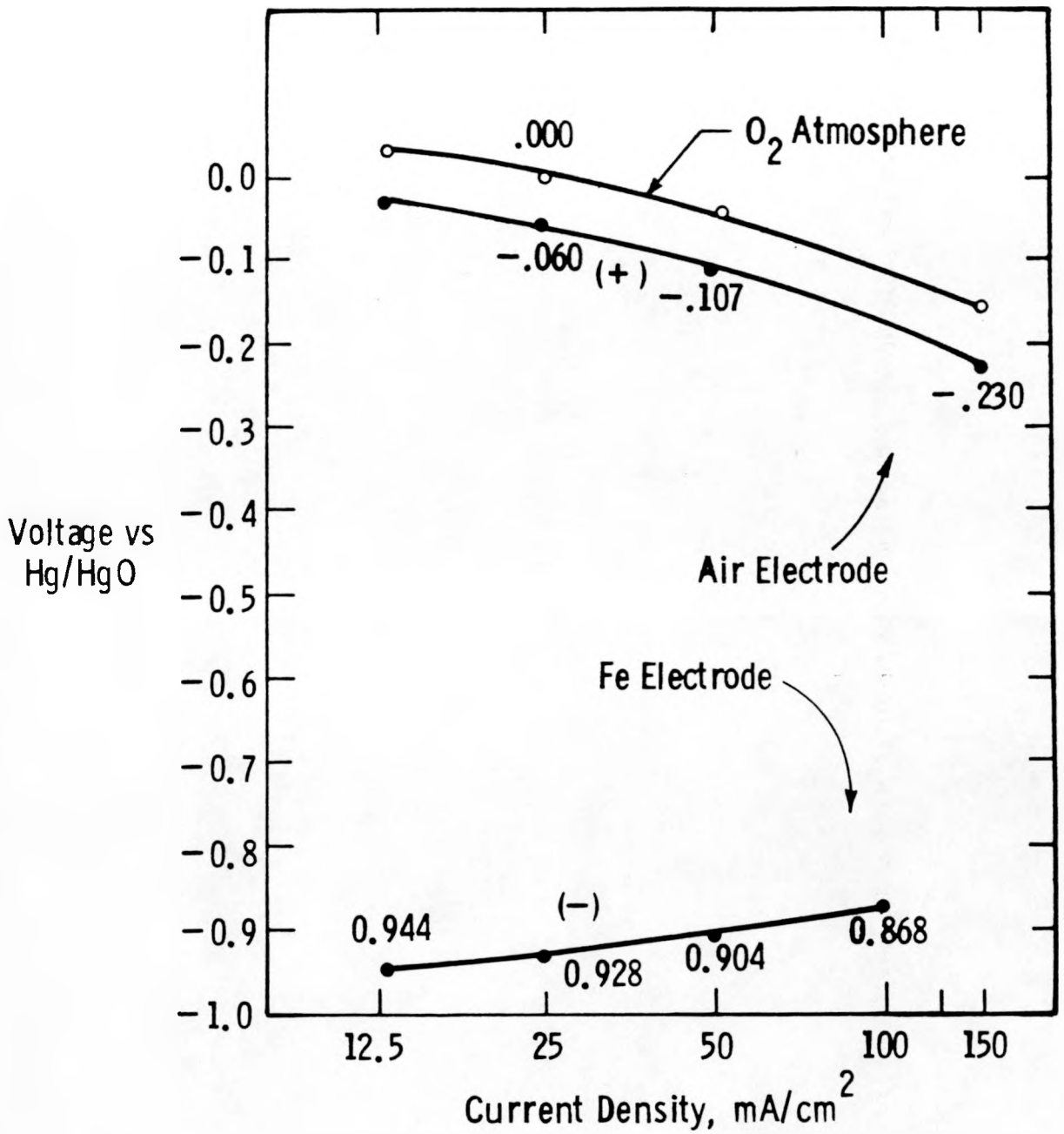

Figure 5-1: Electrode Polarization Characteristics

Figure 5-2 compares the performance characteristics of three 100 cm^2 cells tested at 44°C in a CO_2-free chamber. Cells #30 and #35 employed similar iron electrodes but contained different air electrodes. Though cell #36 was cycled routinely on scrubbed air, one cycle was run with the chamber filled with flowing oxygen gas. Both cells, #30 and #35, show acceptable voltage-current characteristics. Cell #36 shows the expected 60 mV improvement with pure oxygen. One important comparison between cell #36 and #35 is the shape of the polarization curve. Cell #35 and #36 have essentially the same shape, different only by the 60 mV activity difference for oxygen and air. There is no indication of a diffusion limit with air at the higher current densities when compared to oxygen under the same current density conditions.

Figure 5-3 shows that data presented in Figure 5-2 represented as the power delivered by the iron-air couple for the three cells as a function of current. It can be seen from these curves that even at a cell current density of 200 mA/cm^2, peak power has not yet been achieved. In order to more realistically appraise these power curves, the data point for cell #35 at a current density of 200 mA/cm^2 and a terminal voltage of .570 volts was used in a design calculation of what this would translate to in an electric vehicle cell. In terms of a projected 400 cm^2 cell with the expected design goals achieved for the cell case and electrolyte, the cell would deliver 80 watts per kilogram. Our ultimate goal for the iron-air cell is to deliver in excess of 100 watts per kilogram. We expect that by proper cell design and with the expected improvements in scale-up that the internal cell impedance will be reduced, resulting in an improvement in the cell power characteristics. From Figure 5-3 we can determine the cell impedance between the voltage at 10 amps and the voltage at 20 amps. At 10 amps the cell voltage was .700 volts, while at 20 amps the voltage was .570 volts. Therefore, the cell impedance is the voltage difference divided by the current difference or (.700 - .570) volts divided by (20-10) amperes or .130/10 = 13 mΩ. A reduction of this cell impedance from a value of 13 mΩ for a 100 cm^2 size cell to 10 mΩ would provide cell power characteristics well in

Curve 693231-A

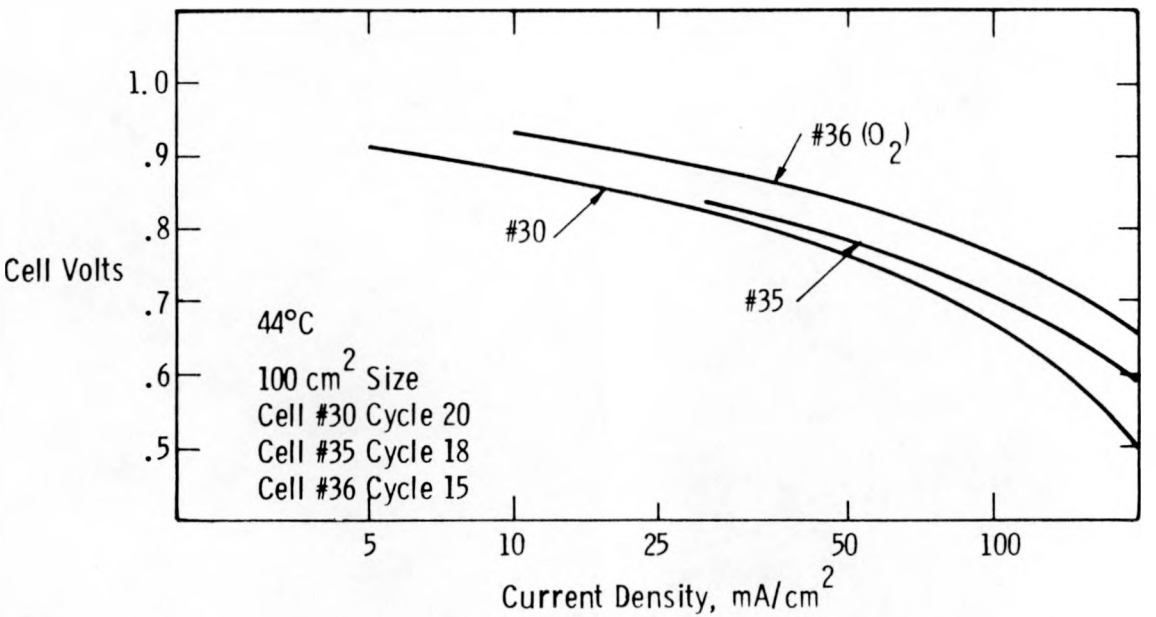

Fig. 4 – Discharge polarization characteristics of several iron-air cells

Figure 5-2: Iron-Air Voltage Characteristics

Curve 694585-A

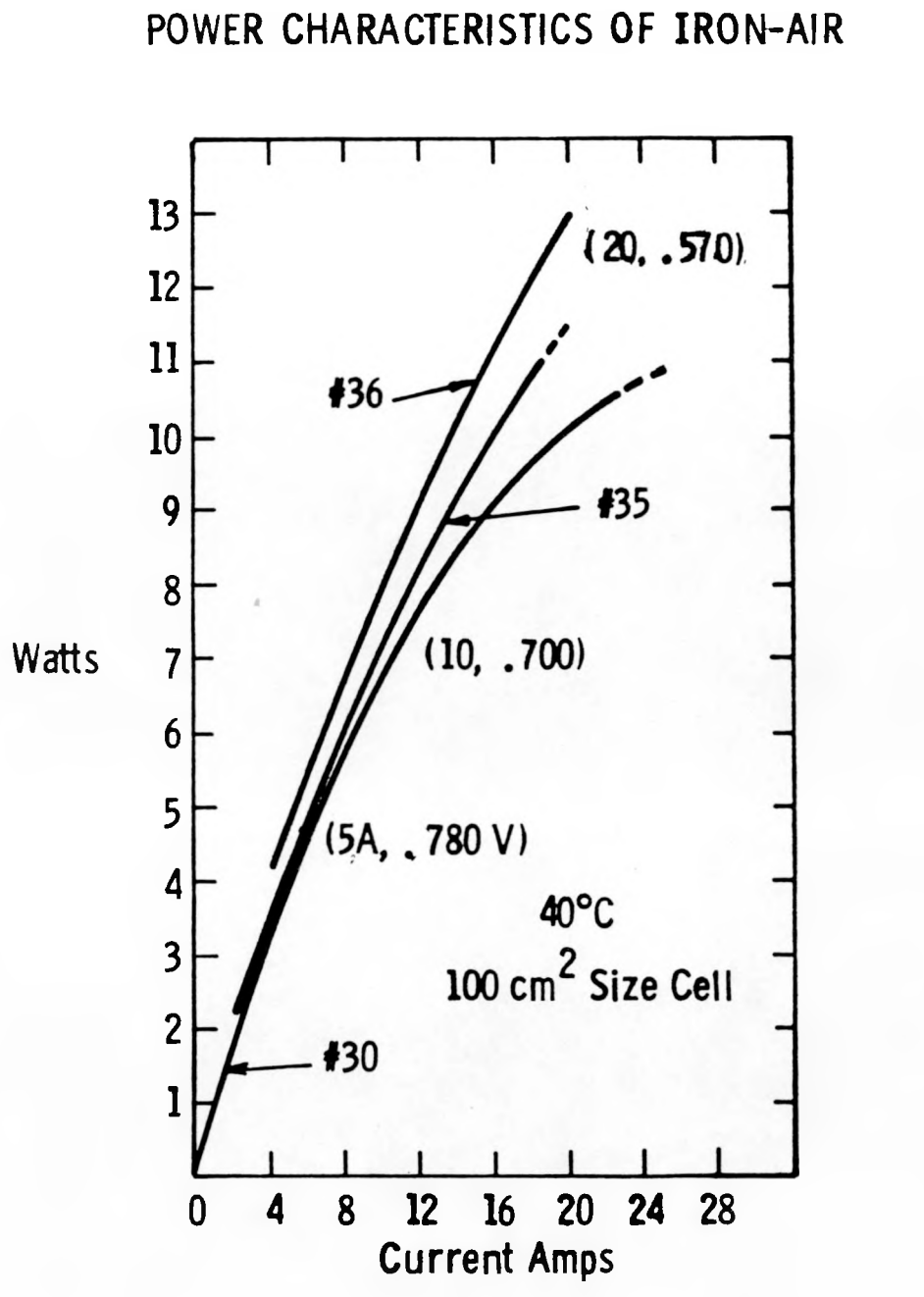

Figure 5-3: Power Characteristics of Iron-Air Cells

excess of our projected goal of 100 watts per kilogram. In terms of a projected 400 cm^2 size cell, we would expect the cell impedance to be less than 2.5 mΩ. These results should be achievable by suitably designing the cell to minimize both resistance and polarization losses.

Figure 5-4 shows the cyclic voltage characteristics of cells tested during the last half of 1977 as they compare to cells tested during 1975-76 and our expected goals. During the era 1975-76, typical cell charging voltages were between 1.7 and 1.8 volts. Recently, cells have displayed charging voltages of 1.6 volts and less at the eight hour charge rate. In the discharge mode, typical cells during 1976 were experiencing terminal voltages of around .7 volts. Recent cells, like #30, #35 and #36 have had terminal discharge voltages of .8 - .83 volts at the four hour discharge rate. In terms of cyclic voltage efficiency, these cells were in excess of 50% efficiency.

The energy efficiency of these cells was low due to the charging regime which intentially had excess charge put into the cells by the cycler. Previous results with high capacity iron electrodes in half cells have shown charge acceptance characteristics in excess of 90%. If we assume that this performance characteristic can be duplicated in cells, the iron air cell will have a cyclic energy efficiency in excess of 45% and may approach 55% with further improvements in electrode technology and improved cell design.

The life characteristics of the cells tested to date, were essentially limited by mechanical assembly problems. Only recently have we made cells which can be cycled to demonstrate electrode characteristics without the mechanical and structural short-comings. Cells tested to date have accumulated over 100 cycles. Table 5-II summarizes the performance of the cells tested, with their total number of cycles and the cause of failure.

Curve 693230-A

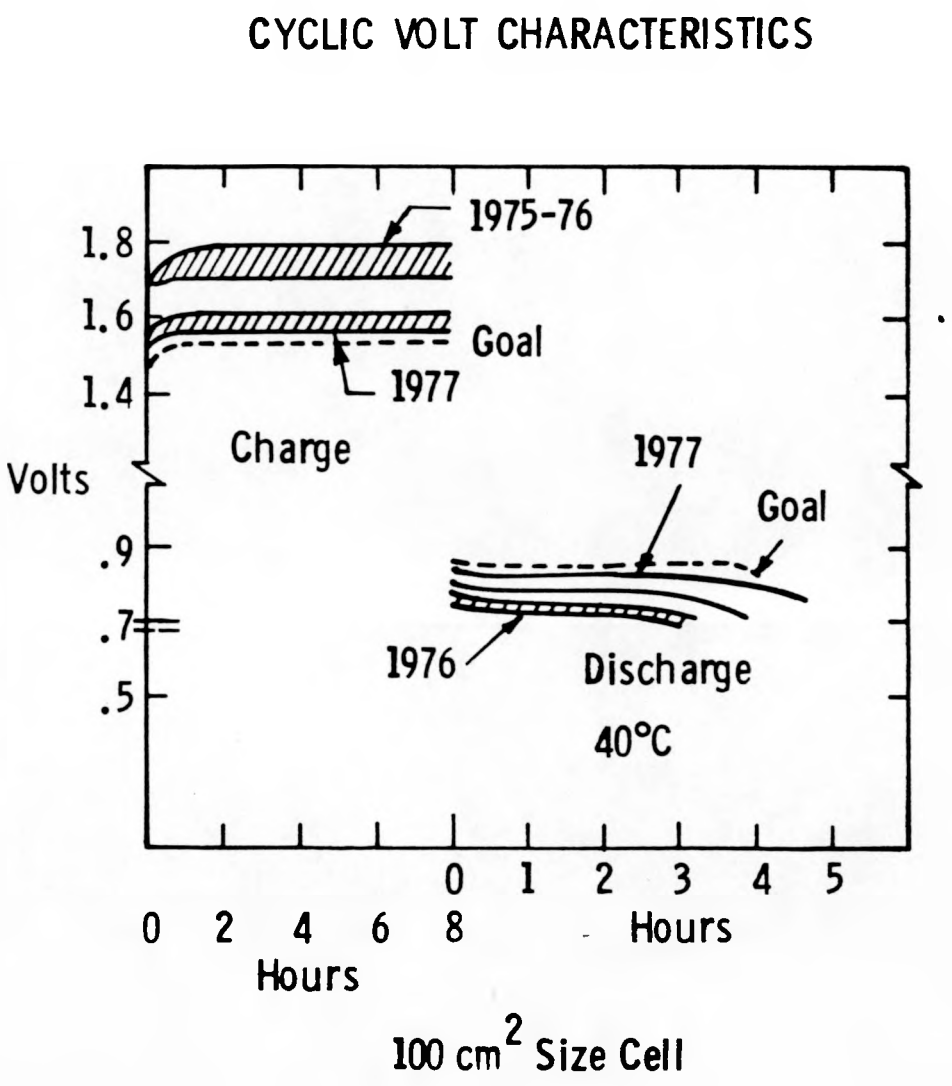

Figure 5-4: Cycle Voltage Characteristics

Table 5-II

Cell No.	Date on Test - Off Test	Total Cycles	Failure
50	1-19-78 1-23-78	6	Leak
51	1-19-78 3-20-78	122	Leak
39	2-2-78 3-21-78	115	Leak
40	2-2-78 3-21-78	105	Leak
44	2-2-78 3-13-78	103	Leak
57	2-13-78 2-23-78	32	Leak
58	2-24-78 3-2-78	6	Leak
62	3-3-78 3-20-78	24	Leak
41	3-28-78 4-19-78	33	Leak
42	3-28-78 4-19-78	33	Leak
54	3-28-78 3-31-78	7	Leak
66	3-28-78 3-29-78	3	Leak
68	3-28-78 4-18-78	33	Leak
70	5-8-78 5-15-78	9	Low Capacity
73	5-12-78 5-18-78	4	Low Capacity
72	5-16-78 5-17-78	1	Shorted
71	5-24-78 5-25-78	2	Low Capacity
Parallel Cells	Fe-Air - Module #1		
63	3-21-78 3-29-78	5	Leak
64	3-21-78 3-29-78	5	Leak
67	3-21-78 3-29-78	5	Leak
Parallel Cells	Fe-Air - Module #2		
74	4-20-78 4-26-78	2	Leak
75	4-20-78 4-26-78	2	Leak

5.4 Module Design and Testing

Two, 100 cm^2 module design concepts were built and evaluated to determine both performance and problems involved with parallel connected cells. The initial cell, or module, consisted of two air electrodes connected in parallel with a common air chamber with two counter iron electrodes connected in parallel. The particular module was built to investigate the electrical characteristics of the configuration. The module had an air supply and electrolyte circulating system attached to simulate expected use conditions. This particular module did not display the expected low impedance characteristics for parallel connected air electrodes. The impedance was approximately 50% higher than anticipated. The continued testing and detailed investigation of this module was terminated due to mechanical problems which led to electrolyte flooding of the air chambers.

A second 100 cm^2 module was designed using three air chambers with four air electrodes connected in parallel with three parallel connected iron electrodes. Once again, mechanical problems forced premature termination of the module testing before any reliable performance data could be acquired for evaluation. It was apparent from the limited amount of data that was collected that the electrical characteristics of the system were not behaving as expected based on the design concept. In particular, the overall impedance of this three-chamber module was off by 100% over expected results. These impedance problems, as they relate to the design of the iron-air module, must be studied in greater detail. The first preliminary attempts at connecting iron-air cells in parallel exhibited unexpected problems which must be studied in much greater detail as we proceed into the module development phase of the iron-air development program.

5.5 Energy Efficiency of Iron-Air Cells

The cyclic voltage efficiency of the iron-air system is controlled primarily by the voltage characteristics of the bifunctional air electrode. In the discharge mode the air electrode reduces oxygen from air at about 100 mV below a Hg/HgO reference electrode at 25 mA/cm^2. At this current density, which is the expected electric vehicle cruise condition, the iron electrode's potential is about 930 mV below Hg/HgO. The cell potential, at the cruise condition is then 830 mV. In the charge mode, the bifunctional air electrode evolves oxygen at about 500 mV above a Hg/HgO reference electrode at 12.5 mA/cm^2 or the eight hour charge rate. The iron electrode potential at the eight hour charge rate is about 1.05 volts below a Hg/HgO reference electrode. The cell potential at the eight hour charge rate is about 1.55 to 1.57 volts. These charge-discharge voltage characteristics are shown schematically in Figure 5-4 as the voltage levels have changed over the development period. Typical cell voltage efficiencies for state-of-the-art cells have been 53% (1.57 volts charge/.83 volts discharge). It is expected that this voltage efficiency can be improved to 60% by decreasing the oxygen overpotential in the charge mode while also improving the oxygen reduction voltage.

The coulombic efficiency of the iron-air system is dictated by the charge acceptance character of the iron electrode. Cyclic efficiencies of greater than 90% for various iron electrodes have been observed. When coupled with the cyclic voltage efficiency of the system, the total iron-air electrochemical couple could have an ultimate system efficiency approaching 60%. Decreases in the system efficiency will occur when more realistic cyclic conditions are employed, namely, those associated with the expected commuter electric vehicle mission.

VI. APPENDIX Iron Electrode Model

The full charge (theoretical) upper plateau discharge capacity for a fully dense iron electrode is 7.55 A·hr/cm^3 (0.962 A·hr/gm x 7.86 gm/cm^3). This value, which could be realized if the molar volumes of iron and its discharge product, $Fe(OH)_2$, were equal, is shown as point A in Figure 4-27. For the condition of zero density (100% initial porosity) the discharge capacity is naturally zero (point B of Figure 4-27). The line connecting points A and B describes the full charge capacity as a function of percentage of initial porosity in the electrode (P). If the volume of the current collector is considered (about 5 to 6% of the total electrode volume) the dashed full charge capacity line is obtained.

To determine the actual maximum capacity for any given initial porosity, it is necessary to consider the difference in molar volumes between iron ($\bar{V}_{Fe}$) and $Fe(OH)_2$ ($\bar{V}_{Fe(OH)_2}$ and to formulate an expression for the change in percent of theoretical capacity (ΔQ) with respect to the change in porosity (ΔP) which occurs during discharge. The needed expression, according to Selanger,[2] is

$$\frac{\Delta Q}{\Delta P} = \frac{\bar{V}_{Fe}}{(\bar{V}_{Fe(OH)_2} - \bar{V}_{Fe})} \qquad \text{(VI-1)}$$

Substitution yields a $\Delta Q/\Delta P$ value of 0.35. A number of discharge lines having this slope are shown in Figure 4-27. For line (1), for example, the electrodes initial porosity is 70%. By discharging along the "discharge" line until all of the porosity is filled, a maximum capacity is realized which corresponds to the difference in ordinate values for the points P = 70 and P = 0. The initial porosity of 70% is not great enough to contain all the $Fe(OH)_2$ that would have formed had a complete upper plateau discharge been possible. By similar reasoning, an initial porosity of 90% (discharge line 2) is too great. At the completion of upper plateau discharge a large amount of porosity remains unfilled because of the low proportion of iron to initial porosity. Only for an initial porosity of about 78% (discharge line 3) is the optimum condition found, i.e., the full upper plateau capacity is realized and the total porosity is utilized.

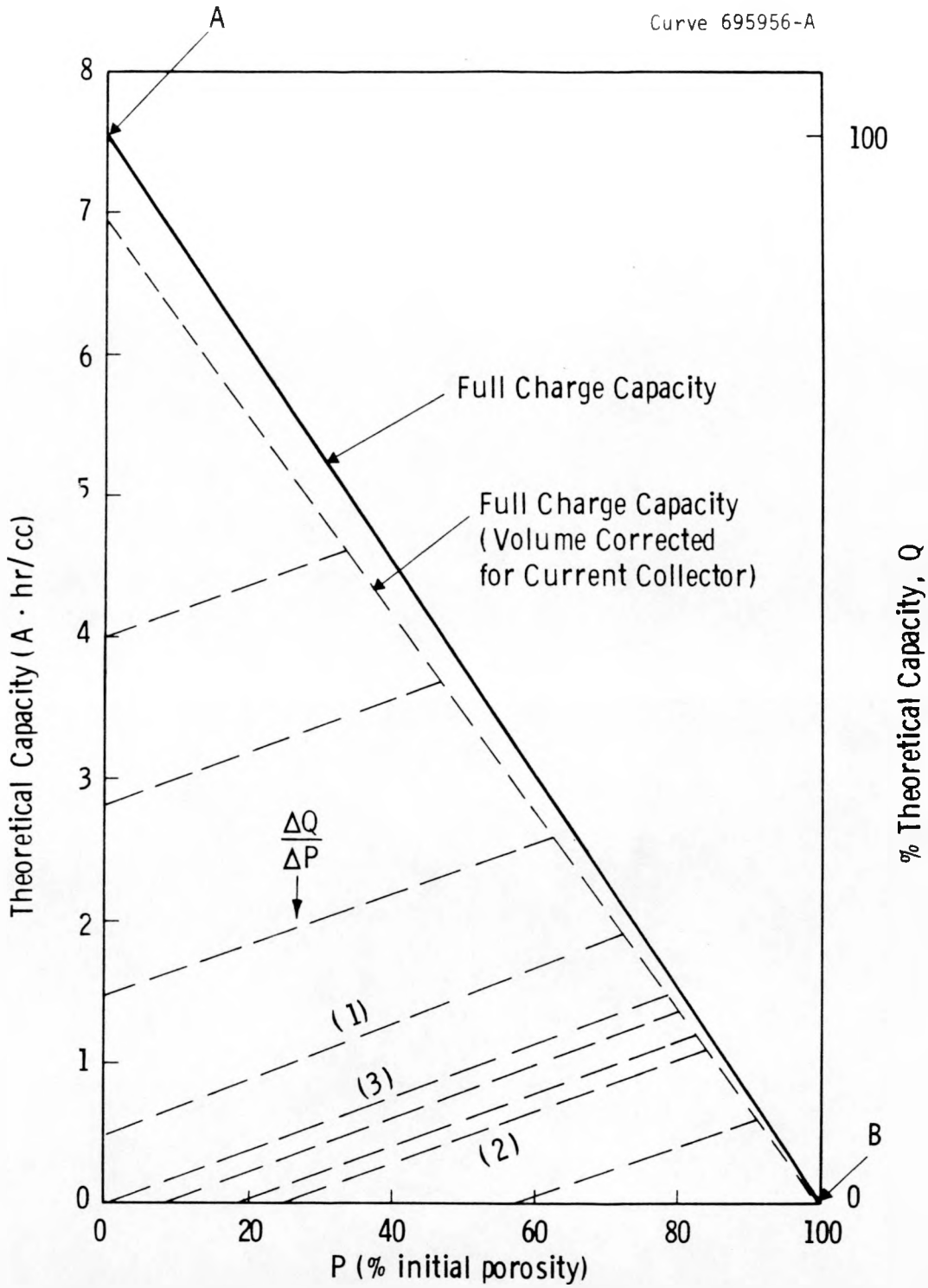

Figure 4-27. Model Constructed to Determine an Iron Electrode's Maximum Capacity as a Function of its Initial Porosity.

By similarly obtaining the maximum capacities corresponding to a number of initial porosity values, the plot of Figure 4-2 was obtained. Conversion of the capacities from a volume to an active weight basis provided the data necessary for the construction of Figure 4-3.

VII. REFERENCES

1. Buzzelli, E. S., Iron-Air Battery Development Program-Interim Report June 1976-June 1977, Report # COO/2949-1 (September 1977).

2. Selanger, P., J. Appl. Electrochemistry, 4 (1974) 263.

3. Gallagher, P. K., D. W. Johnson, Jr., and F. Schrey, Ceramic Bulletin, 55 (1976) 589.

4. Mitsumata, T., et al., Japanese Unexamined Patent Application No. 51-113129 (October 6, 1976).

5. Fukuda, M., T. Iwaki and T. Mitsumata, U. S. Patent 3,847,603 (November 12, 1974).

6. Turkdogan, E. T., R. G. Olson and J. V. Vinters, Met. Trans., 2 (1971) 3190.

7. Kuczynski, G. C., Tr. AIME 185 (1949) 169.

8. Fischmeister, H. F., and R. Zahn, Modern Developments in Powder Metallurgy (H. H. Hausner, ed.), Plenum, New York (1966) p.12.

9. Poster, A. R., and H. H. Hausner, in Modern Developments in Powder Metallurgy (H. H. Hausner, ed.,) Plenum, New York.

10. Fedorchenko, I. M., and I. I. Ivanova, Soviet Powder Metallurgy and Metal Ceramics, 84 (1969) 23.

11. Vassie, P. R., and A. C. C. Tseung, Electrochimica Acta, 21 (1976) 299.

12. Öjefors, L., Report-Studies on the Alkaline Iron Electrode, Swedish National Development Company (August 1975) p. I-9.

13. H. A. Hancock and J. A. Strasser, in Modern Developments in Powder Metallurgy, 1974 (H. H. Hausner, ed.), Plenum Press, N,Y., 13.